Petroleum Science 22 (2025) 1021–1040

Contents lists available at ScienceDirect

Petroleum Science

journal homepage: www.keaipublishing.com/en/journals/petroleum-science

Original Paper

Morpho-dynamics in fan deltas: Effect of topography on flow transformation, facies distribution and graded profile evolution, a case study in XLG fan delta

Hong-Wei Sun [a], Shun-Li Li [a,*], Pan Li [b], Chao-Fan Wei [a], Zhan-Teng Wu [a], Long-Jv Hai [a]

[a] School of Energy Resources, China University of Geosciences (Beijing), Beijing, 100083, China
[b] Research Institute of Petroleum Exploration and Development, PetroChina, Beijing, 100083, China

A R T I C L E I N F O

Article history:
Received 1 September 2024
Received in revised form
10 December 2024
Accepted 31 December 2024
Available online 11 January 2025

Edited by Jie Hao

Keywords:
Fan delta
Flow transformation
Facies distribution
Lobe stacking
Graded profile
Base level

A B S T R A C T

Fan deltas are usually constructed through episodic flood event with debris flow transforming to hyper-concentrated flow during sediments proceeding. However, the role of topography in controlling the flow transformation and sediments aggradation has been less studied. This constrain studies of sediment distribution and understanding of graded profile. For lake basin sequences, geomorphological control is much stronger than lake level rise and fall. Under extreme conditions, sediments can still prograde when the lake level rises. Therefore, describing the influence of geomorphology on the flow transformation and stacking pattern of the lobes can provide a deeper understanding of the controlling factors of the lake basin stratigraphy sequence. Xiligou lake (XLG) fan delta from Xisai Basin provides an optimal case for addressing this issue. Three lobes developed on the XLG fan delta with significant differences in their morphologies, architectures, lithofacies, sediment distributions and topographies. Through trenching, drone photography, and satellite data, we analyzed the structure of the sediments and the distribution of sedimentary facies. Based on the analysis of debris flow and hyper-concentrated flow deposits, two transformation models corresponding to different topographies were established. Sediment unloading is caused by a frictional reduction or a sudden momentum loss in the sediments flow's carrying capacity, allowing the debris flow transforms to hyper-concentrated flow and then to stream flow during the movement. The role of topography in controlling sediment flow transformation and sediment distribution is clarified through forces analysis of sediment grain. The topographic gradient of the linear slope is constant, so the direction of fluid movement is consistent with the topographic direction. Therefore, sediment flows move on linear slope without collision with the bed and there is no sudden loss of momentum. The gradual or sudden reduction in topographic gradient of concave slopes forces a constant or sudden change in the direction of fluid movement, which facilitates the unloading of sediments and the transformation of flow. The sudden change of topography forces unloading of viscous component, and the non-viscous component pass over to form hyper-concentrated flow, often accompanied by remobilized large gravels. The graded profile was an equilibrium between the dynamics and resistance of sediment transport. Changes in lake level affect the graded profile by changing the elevation of sediment transport, which is the total gravitational potential energy. The instantaneous graded profile and temporary graded profile are different scales of equilibrium corresponding to hydrodynamic equilibrium and depositional trend respectively. This study reveals the role of geomorphological dynamics in controlling sedimentary body progradation, thus providing a new perspective on the analysis of lake basin stratigraphy sequence.

1. Introduction

Fan deltas, defined most commonly as an alluvial fan that has prograded from an adjacent highland into a standing body of water, either a lake or the sea (Holmes, 1945), are crucial landforms

* Corresponding author.
E-mail address: lishunli@cugb.edu.cn (S.-L. Li).

https://doi.org/10.1016/j.petsci.2024.12.028
1995-8226/

formed by episodic flood events which involve the transformation of debris flow into hyper-concentrated flow as the sediments progress (Postma, 1990; Nemec, 1990; Kataoka and Nakajo, 2004). It also plays a significant role in sediment routing systems between subaerial and subaqueous deposition (Prior and Bornhold, 1990; Allen, 2008, 2017; Li et al., 2017a, 2017b; Yang et al., 2020). For hybrid-event beds, clarifying the sediment flow transformation in fan deltas can provide new understanding of trigger mechanisms of deep-water turbidite systems (Fonnesu et al., 2018; Baas et al., 2021b), especially in the context of the topography-controlling effect on sediment gravity flows (Tinterri et al., 2020; Shanmugam, 2020; Guo et al., 2021).

Fan delta is mainly composed of debris flow and hyper-concentrated flow finally shifting to stream flow (Postma, 1990; Nemec, 1990; Kataoka and Nakajo, 2004). The investigation on debris flow and hyper-concentrated flow deposits has led to the establishment of transformation models. Sohn et al. (1999) proposed two models of debris flow transforming to hyper-concentrated flow based on researches on an alluvial fan. One model described a hyper-concentrated flow generated by the dilution at the leading edge of a debris flow that entered a river valley. And the other illustrated a debris flow preceding in advance of a hyper-concentrated flow and streamflow. Both models led to the same distribution with debris flow deposits at proximal, hyper-concentrated flow in the middle, and stream flow at distal. A lot of subaqueous models of gravity flows have been established due to sediments distribution, but limited attention has been given to the role of topography in fluid process (Pierson and Scott, 1985; Zavala, 2020; Kvale et al., 2020; Yang et al., 2020).

Transformations of sediment gravity flows, pertaining to transition between laminar and turbulent flow, is controlled by parameters such as sediment concentration, flow thickness and velocity, as well as topographic slope gradient (Baas et al., 2009, 2011), which can be attributed to the interaction between topography and flow with sediments exchanging. The controls of topography on an alluvial-fan delta system have received increasing attention: (1) Topography provide the principal driving force of sediments transportation, and the competition between driving force and resistance during transporting (Gao et al., 2019; Hussain et al., 2020). (2) It controls the morphology of fan delta through governs acceleration or deceleration and orientation of sediments flow (Harvey et al., 2005). As long as shear stresses are well above critical which can be maintained by enough steep slope, the impact of water flux on fan morphology is much stronger than grain size (Parker et al., 1998). (3) In the meantime, fan slope is dependent on discharge and sediments illustrated by flume experiments (Whipple et al., 1998; Milana and Ruzycki, 1999; Milana and Tietze, 2002; Zhang et al., 2021), numerical models (Parker et al., 1998; Geleynse et al., 2011; Nota et al., 2024), and field investigations (Bull, 1964; Gao et al., 2019, 2020). These findings underscore the critical influence of topographic features in shaping sedimentary processes and highlight the significance of detailed topographic mapping in understanding sediment dynamics and distribution.

Therefore, this paper will rely on satellite remote sensing and UAV tilt photography to establish a topographic model. Characterize the spatial distribution of lithofacies and hydrodynamic changes of interpreted sediments flow based on sedimentary structures showing on satellite and UAV images and field observations (Baas et al., 2021a, 2021b). From the perspective of force analysis, moving simulation and stratigraphy, we will explain how the topographic slope affects the fluid flow transformation process and stacking pattern of the lobe.

2. Geological backgrounds

2.1. Tectonic setting

XLG lake is located in Ulan County, Qinghai Province, in the northwestern part of Qinghai-Tibet Plateau, about 100 km due west away Qinghai Lake. The lake surface is about 2934 m above sea level, and the lake area is about 20 km^2. XLG Lake is situated in the narrow NWW-oriented Xisai Basin, in the eastern margin of the Tsaidam Basin, which is a faulted basin confined by retrograde faults between mountains on a thrusting body (Lv, 2018), with several positive fault-cut blocks. A positive fault inclined to a dip of 30° due north develops at the root of the fan delta body.

2.2. Climate and hydrogeological conditions

The Dulan River and the Saishek River are two main recharge rivers in the basin. The Saishek River originates in the Ulanbeyli and Goerel Mountains in the north of the basin, with a total length of 45 km and a catchment area of about 965 km^2. The source of the Dulan River is located in Guanjiaozhigou and Goerel Gou in the Tsakhano Depression, with a catchment area of about 501.25 km^2. The two rivers show a scattered flow after leaving the mountain pass. Some of the river water is directly recharged to groundwater by infiltration in the pre-mountain area, and at the alluvial fan. It gushes out of the ground in the form of springs to form swamps and spring streams, and finally all of them converge in the XLG Lake (Lv, 2018).

Wulan-Duran area is a typical semi-arid and alpine climate area of the inland plateau, controlled by high-pressure westerly winds and the influence of Mongolian-Siberian anticyclones, showing typical continental climate characteristics, dry, low rainfall and windy, with long and cold winters, short and cool summers, annual solar radiation of 1577~1777 MJ/m^2. Precipitation in the plains ranges from 37.9 to 180.5 mm, concentrated in May–September. The low temperature in January is −15 ~ −10 °C, the high in July is 9–19.3 °C, the lowest temperature is −39.2 °C, the highest temperature is 33.9 °C, the daily difference is 12.6 °C, and the annual difference is 23.9–29.7 °C, which is greater in the west than in the east. The region is an arid area, with a humidity coefficient of 0.21–0.35, annual evaporation of 2049.6 mm, annual sunshine hours of about 3100 h, and average daily sunshine hours up to 7–10 h throughout the year (Chen et al., 2016) (Fig. 1(d and e)). Climate controls lake-level fluctuations through the balance between precipitation and evaporation (Uhrin and Sztan'o, 2012; Woolway et al., 2020), which governs sediment supply and fan morphology indirectly through weathering of source areas and vegetation (Nelson et al., 2009; Evangelinos et al., 2017). Precipitation and temperature in this region vary in cycles of about 10 years and annual rainfall is concentrated in summer and scarce in winter (Fig. 1(d and e)), making XLG fan delta formed by intermittent flooding.

2.3. Catchment and fan morphology

Reading and Richards (1994) classified fans as a point source and a lineal (multipoint) source according to the different control of the faults on the source of the fan. The "Y"-shaped fault developed in the south Maoniu mountain of the XLG Lake, forming a single vent between the fault blocks, which allows the source to emerge from the outlet in a "point" pattern (Fig. 1(a)).

The sediments of the XLG fan delta are derived from two catchments. Source area A in the east is mainly volcaniclastic rocks of the Upper Ordovician, granodiorite and diorite of the Hercynian and granite of the Indo-Chinese, with a maximum elevation of

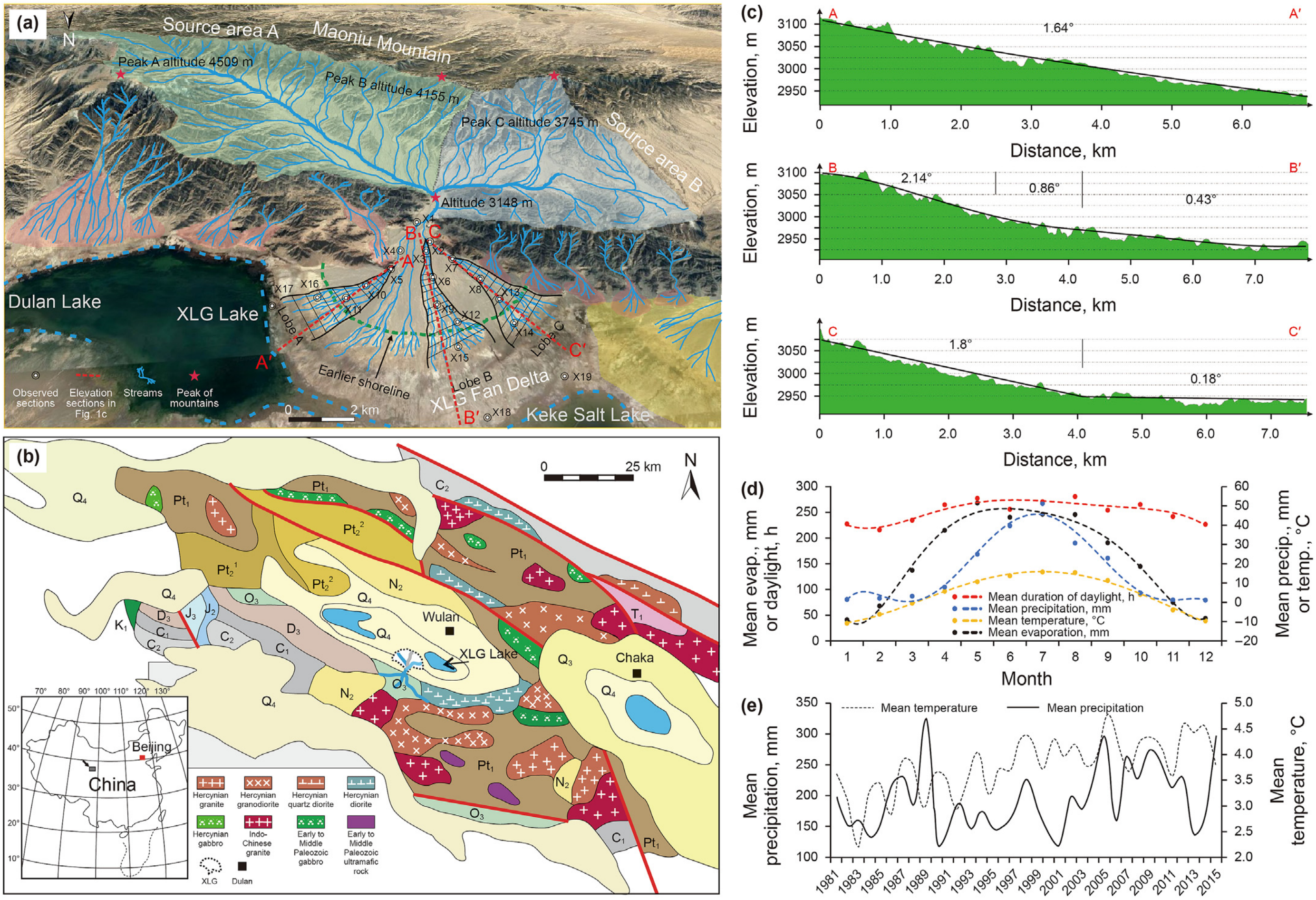

Fig. 1. Geological setting of the XLG Fan delta. **(a)** Satellite image showing the study area and locations of measurements. **(b)** Regional geological map (modified from Qinghai province geological map 2016). **(c)** Longitudinal topographies of different lobes. **(d)** Monthly variations in regional mean precipitation, mean temperature, mean daylight and mean evaporation of the Wulan country (data from Shi and Xiao, 2003; Luo and Wang, 2017; Chen et al., 2016). **(e)** Yearly variations in regional mean precipitation and mean temperature of the Wulan country (data from Luo and Wang, 2017).

4155 m above sea level, an area of 86.9 km^2, and an average slope of 10.2°. Source area B in the west is dominated by volcaniclastic rocks of the Upper Ordovician, and clastic rocks of the Upper Devonian and Upper Neogene, containing abundant flesh-red granite conglomerates, with a maximum elevation of 3745 m above sea level, an area of 22.5 km^2 and an average slope of 4.3° (Fig. 1(a and b)).

Covering an area of about 48 km^2, the XLG fan delta is the largest one of fan systems along the basin margins, showing a symmetrical fan shape with a center angle of 117.5°, a maximum radius of about 7.4 km, a maximum width of about 9.6 km, and an average slope of 1.6°. Contiguous alluvial systems have developed in the adjacent areas, with several alluvial fans overlying the XLG fan delta in the west part (Fig. 1(a)).

Three sedimentary lobes that had been recently active were developed on the surface of the fan delta showing a lighter tone on satellite images. The darker area is the product of oxidation over long intermittent periods of deposition, while the lighter areas are those currently active. The envelope of the still active region can then be used as the boundary of the lobe (Blair and McPherson, 2009; Harvey, 2011; Bahrami et al., 2015). Their shapes, as well as the development of the watercourses are significantly different. DEM elevation data shows the differences in the longitudinal topographic variations of the three areas. The slope of the lobe A is a constant value of 1.64°. The slope of lobe B shifted gradually from 2.14° to 0.86° and finally to 0.43°. The slope of lobe C has two segments connected by a knickpoint, which is 1.8° and 0.18° respectively (Fig. 1(a–c)). The differences between the three slopes are due to the uneven accumulation of different grain-size sediments. Each lobe carries different composition of sediments, with different flow regimes and different spatial erosion or deposition. In terms of angle of repose, it increases with increasing grain size (Lane, 1953; Wu et al., 2017). Therefore, areas with steeper slopes may have higher gravel content and larger grain sizes. Through the analysis of facies and sediments distribution, the geomorphological control on sedimentation will be revealed.

3. Data and methods

A field expedition was conducted to provide detailed profiles of 19 sites in total within the XLG fan delta. The studied locations are mainly distributed along the cliff sections of the incised valley range from 10 to 150 m in length and 1–2 m in height. Additionally, 6 trenches, about 0.5 m high, were excavated to expose transverse sections from the proximal to the distal fan (sections 14 to 19 in Fig. 1(a)) to better characterize the downslope and lateral variability of architectures and facies of XLG fan delta. Typical samples were collected for grain-size and grading analyses. A total of 17.74 m of sedimentary logs were measured at a 10 cm resolution and correlated to understand the spatial changes in the style of sedimentation.

The analysis of lithofacies and their associations, as well as the accumulation probability curves of grain size, allowed for the examination of the transformation of flow regime. The plane distribution of channels and bars were observed using satellite maps and UAV flat tilt photography. Width of lobes, the width and number of bars were characterized and measured. The topographic variations of different lobe depositional areas were obtained through DEM elevation data at a 30 m resolution downloaded from Geospatial Data Cloud. Finally, equations and models were established to discuss the controlling effect of topography on sediment distribution through the transformation of flow regime and energy, from the perspective of morpho-dynamics, which is the interaction of topography, flow regime, and consequential sedimentary facies.

4. Results

4.1. Facies and interpretation

4.1.1. Debris flow deposits

4.1.1.1. Description. Cohesive debris flow deposits are disorganized cobble to boulder conglomerates with a maximum diameter of 70 cm, subrounded to rounded, poorly sorted. They are matrix supported with clasts floating in coarse sands or fine gravels. Inverse grading, with high dip angle clasts even uptight. And the dip angle becomes smaller from bottom to top, which indicates a rolling effect of bottom pebbles to weaken the friction from bed and a dispersive pressure support for top cobbles (Table 1, D1). Non-cohesive debris flow deposits lack sand deposits. They are disorganized or weakly organized cobble to boulder conglomerates with a mean diameter of 30 cm, clast supported, poorly to moderately sorted. Clasts oriented in low dip angle, weakly imbricated, without obvious grading. There would be outsized clast floating in finer pebbles (Table 1, D2; Fig. 2(a)).

4.1.1.2. Interpretation. The mechanics of debris flows involve friction and momentum transfer between coarse-grained materials, electrochemical reactions between fines, and physical reactions between the fluid, sediment grains and the bed (Brenna et al., 2020). The interpretation of debris flow deposits has been mainly based on the viscoplastic flow model (Johnson, 1970, 1984) and the inertial grain flow model (Takahashi, 1978, 1981). Both models suggest that the deposition of a debris flow takes place by mass freezing when the driving shear stress falls below the yield strength of the viscoplastic material with disorganized clast fabrics or when the dispersive pressure drops and the grains become frictionally bound with preferred clast orientation (Enos, 1991; Lewis et al., 1980), corresponding to cohesive and non-cohesive debris flows (Lowe, 1979, 1982; Nemec and Steel, 1984). Some debris flows can even exhibit turbulence and their deposits exhibit normal grading (Lowe, 1982) and scour surfaces (Gao et al., 2019).

4.1.2. Hyper-concentrated flow deposits

4.1.2.1. Description. There are three types of hyper-concentrated flow deposits. (1) Disorganized cobble to gravel conglomerates and sands with a maximum diameter of 30 cm, subrounded to rounded, poorly sorted, massive sand and fine gravels laying on top. They are matrix supported or clast supported. Normal grading, with oriented in low dip angle, weakly imbricated. Outsized clast may show high dip angle even uptight (Table 1, H1; Fig. 2(b)). (2) Oriented cobble to pebble conglomerates with a mean diameter of 15 cm, subrounded to rounded, well sorted, clast supported, outsized clast up to 0.2 m. Multiple normal grading bedsets, with bottom pebbles imbricated (Table 1, H2; Fig. 2(c and d)). (3) Stratified pebble to gravel conglomerates, stratified coarse sand with pebble and gravels, subrounded to rounded, well sorted, clast supported, outsized clast up to 0.2 m. Normal grading, gravel oriented and imbricated at the bottom, finer gravels aligned along

Table 1
Characteristics and interpretation of different kinds of sediment flow deposits.

Code	Lithology	Sedimentary structures	Depositional process
D1	Disorganized boulder to cobble conglomerates, subrounded to rounded, poorly sorted, matrix supported, coarse sand to fine pebble matrix. In Fig. 2(a–e).	Massive, structureless or inverse grading, cobble or boulder floating in matrix, large dip angle, even upright.	Cohesive debris flow, mass movement, clasts are supported by buoyancy and dispersive pressures (Johnson, 1970, 1984).
D2	Disorganized or weakly oriented boulder to cobble conglomerates, subrounded to rounded, poorly to moderately sorted, clast supported larger cobble, matrix supported smaller cobble and pebble, outsized clast up to 0.4 m. In Fig. 2(a–e).	Massive, structureless or weakly normal grading, clast supported larger cobble oriented in low dip angle, matrix supported smaller cobble and pebble showed larger dip angle.	Non-cohesive debris flow, mass movement and traction, larger clasts are supported by shearing stress, smaller clasts supported by buoyancy and dispersive pressures (Lowe, 1979, 1982; Nemec and Steel, 1984).
H1	Disorganized boulder to oriented pebble and gravel conglomerates, subrounded to rounded, poorly sorted, matrix supported, coarse sand to fine gravel matrix, outsized clast up to 0.3 m. In Fig. 2 (b).	Massive, normal grading, clast supported larger cobble oriented in low dip angle and imbricated, coarse sands are massive with no obvious structure.	Hyper-concentrated flood flow, high energy, inertial layers and traction, large pebble are dragged by shearing stress, sands and gravels suspended by turbulence (Chen and Zhang, 2015; Brenna et al., 2020).
H2	Oriented cobble to pebble conglomerates, subrounded to rounded, well sorted, clast supported, outsized clast up to 0.2 m. In Fig. 2(c and d).	Massive, multiple normal grading, clast supported clasts oriented in low dip angle and well imbricated, lack sand deposits.	Hyper-concentrated flood flow, lower energy, high turbulence, traction carpets deposits, shearing between layers.
H3	Stratified pebble to gravel conglomerates, stratified coarse sand with pebble and gravels, subrounded to rounded, well sorted, clast supported, outsized clast up to 0.2 m. In Fig. 2(b–f).	Stratified, normal grading, gravel oriented and imbricated at the bottom, finer gravels aligned along lamina	Hyper-concentrated flood flow transforming to traction current, waning traction carpets deposits, shearing between layers.
S1/S2	Trough-shaped and sigmoidal-stratified, or planar-shaped and cross-stratified, well-organized, medium to coarse sandstone with pebble to gravel conglomerate, subrounded to rounded, poorly to moderately sorted, clast-supported. In Fig. 2(g and h).	Trough, planar and sigmoidal cross bedding, erosive bases, multiple bedsets.	Stream flow, traction current, channel deposits or swash deposits by wave.

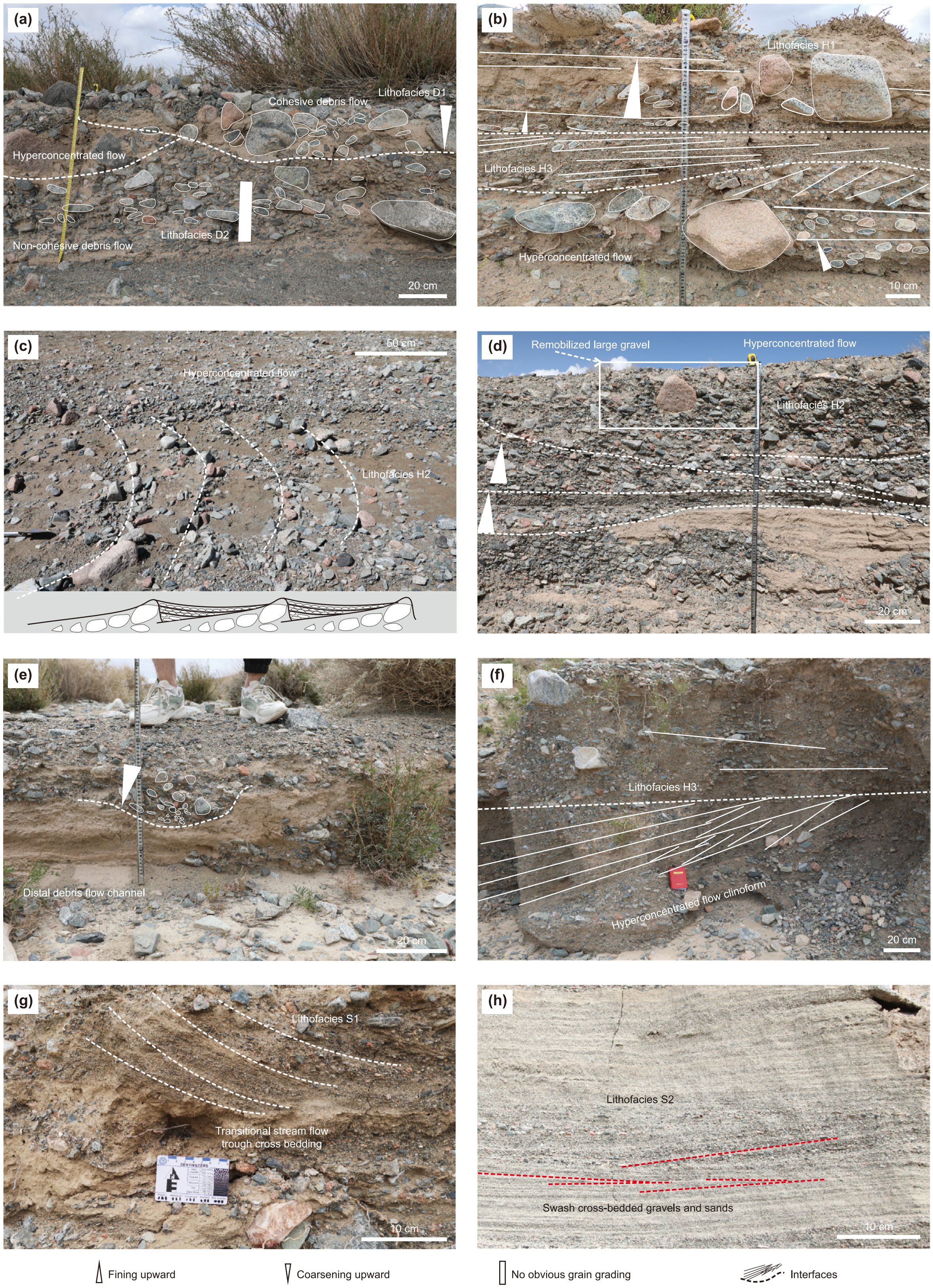

Fig. 2. Typical sedimentary features of the XLG Fan delta deposits. **(a)** Cohesive debris flow deposits and non-cohesive debris flow deposits. **(b)** Hyper-concentrated flow deposits. **(c)** Gravel bedforms formed by hyper-concentrated turbulent flow. **(d)** Frequently interbedded clean conglomerates with few matrices. **(e)** Distal debris flow channel. **(f)** Hyper-concentrated flow progradation of inclined sheet-like layers. **(g)** Trough cross bedding formed by transitional stream flow from hyper-concentrated flow. **(h)** Swash cross-bedded gravels and sands, indicating the wave effect on the sedimentation.

lamina (Table 1, H3; Fig. 2(b–f)).

4.1.2.2. Interpretation. "Hyper-concentrated flow", proposed by Beverage and Culbertson (1964), was defined as an intermediate-type flow between stream-flow and debris-flow. Deposits include dense inertial layers or carpets beneath dilute and turbulent flows (Chen and Zhang, 2015; Brenna et al., 2020) (Fig. 2(b)), forming sheet beds (Nemec and Muszynski, 1982) (Fig. 2(c)), from slightly channelized, weak grading (Fig. 2(d)) (Wasson, 1977; Heward, 1978), to boldly channelized, normal grading (Steel, 1974) (Fig. 2(b)), and even completely stratified (Fig. 2(f)). And because of its high concentration and turbulence, it often carries large gravels from early debris flow deposits downstream (Postma et al., 1988).

The stream flow of the XLG fan delta was transformed from the hyper-concentrated flow and developed at the end of debris surging. Stream flow deposits here, shown on the trench, are massive, thickly bedded and trough cross-bedding conglomerate-bearing sands (Table 1 (S1, S2); Fig. 2(g and h)).

4.2. Facies distribution

There are four kinds of facies developed in three lobes, braided bar, sheet-flooding bar mouth bar and sheet sand. Bar is defined as the positive geomorphic elements including convex deposition braided bar and residual of sheet flooding lobe cut by channels. Braided bar is formed by braided rivers, clast supported, inverse grading. Residual of sheet flooding lobe is usually well stratified, but showing a coarsening upward in multiple bedsets, defined as sheet-flooding bar in this study. The geometry of base level is calculated based repose angles of different-diameter grains (approximated by the coefficient of friction, Hjulström, 1935) and diameter exponential decreasing with distance proposed by Sternberg (1875).

The topography of Lobe A shows a monoclinic character with no obvious topographic changes, and the debris flows, hyper-concentrated flow and streamflow, develop sequentially from proximal to distal ends. In the proximal part of the lobe, at point X4, the debris flow deposits have coarse gravels suspended in sandy or fine gravelly matrix, and in the central part of the lobe, at point X10, the gravels have orientated character with a low angular inclination, suggesting a transition from a cohesive debris flow to a non-cohesive debris flow. The HCF (Hyper-concentrated flow) deposits of Lobe A are predominantly an overlay of fining upward thin gravel layers or small, trough-like, gravels (Fig. 3).

Lobe A exhibits a broom shape in plan, sequentially developing debris flow channel, sheet-flooding bar which is dominated by hyper-concentrated flow, braided bar, mouth bar and sheet sand which is dominated by streamflow. There are regional differences in the distribution of facies. In the western part, braided bars are more developed, while sheet-flooding bars are more developed in the eastern part. Maybe it's because the eastern part is closer to the center of the lake than the western part (Fig. 1). The mouth bars are more developed downstream of the sheet-flooding bars and relatively less developed downstream of the braided bars. This may be due to the fact that the development of the braided bar unloads a large number of sediments, resulting in insufficient residual material carried in the transport medium to form a sizeable mouth bar. In contrast, the sheet-flooding bar unloads only the bed-loaded material from the hyper-concentrated flow, so that most of its suspended substance could unload distally enough to form a mouth bar (Fig. 3).

The topography of Lobe B is characterized by a gradual decrease in slope, with the development of debris flow, hyper-concentrated flow and streamflow from proximal to distal ends. The debris flow sediments show medium to coarse gravel suspended in matrix both proximally and centrally, suggesting that the cohesive debris flow extends further than in Lobe A. The hyper-concentrated flow sediments of Lobe B show more remobilized large gravels and are typified by frequent cross-cutting of medium and coarse gravels in multiple trough-like interbedded laminations (Fig. 4). High proportion non-cohesive debris flow suggests that, unlike Lobe A, debris flows in Lobe B maybe suffer a forced diluting controlled by topography, rather than sedimentary differentiation transforming into hyper-concentrated flow.

Lobe B has a different proportion of facies development compared to Lobe A. Sheet-flooding bars are significantly more developed than braided bars, but both are less developed as mouth bars are more developed than Lobe A (Fig. 4). This is mainly due to less proximal unloading but more unloading at the distal. Moreover, the hyper-concentrated flow of Lobe B re-transported earlier sediments, allowing debris flow deposits to be carried downstream, increasing sediment supply at river mouth.

The topography of Lobe C has two sections, with one relatively steep slope followed by one relatively gentle, and the debris flow, hyper-concentrated flow and streamflow are developed sequentially from proximal to distal end. The debris flow sediments are mainly non-cohesive, gravels oriented at a low angle, with few matrix and suspended gravels. The proportion of hyper-concentrated flow is higher than debris flow at point X2. The hyper-concentrated flow sediments of Lobe C contain more remobilized large gravels and are typified by cross-cutting of medium and fine gravels in multiple trough-like interbedded laminations. At point X13, the stratification of the hyper-concentrated flow sediments becomes less pronounced, with only partial occurrences of small trough-interbedded laminations and thin gravel layers (Fig. 5). This may be caused by the rapid unloading of the hyper-concentrated flow sediments due to the abrupt change in topographic slope.

Compared with Lobe B, Lobe C has a higher proportion of sheet-flooding bars developed, lacks of mouth bars deposits, and mainly develops sheet sand (Fig. 5). This may be due to the abrupt change in topography, which allowed massive unloading of sediments at the knickpoint, resulting in insufficient supply of distal sediments for the formation of large-scale mouth bars. Moreover, it is located in a shallow water area with strong wave action, so that small-scale mouth bars were converted to sheet sand by wave action (Fig. 1).

4.3. Sedimentary parameters

In this part, based on satellite image and UAV planimetric tilt photography, the width of lobes, the width of bars, and the number of bars with distance were measured, and fitted relationships were established respectively. Sediments flow types were classified according to the lithofacies observed in the field profiles, with corresponding percentages calculated and maximum grain size of each observed point measured.

4.3.1. Lobes and bars

The width of Lobe A showed a better linear relationship with distance, while the width of bars showed a slowly increasing and then rapidly decreasing trend with distance. The number of bars behaves similarly, but at the position of 1000 m, the number is unusually low (Fig. 6(a)). This may be due to the fact that after the deposition of coarser particles, the finer remaining particles are in a supercritical state at the prevailing water velocity, leading to a reduction in deposition. The fitting curve of the width of Lobe A and the width of bars shows concave down (Fig. 6(b)), indicating that the effect of bars on the increase of the width of lobe A is greater at smaller but less at larger width of bars. The reason is that the greater the number of bars, the smaller the size at a given sediment

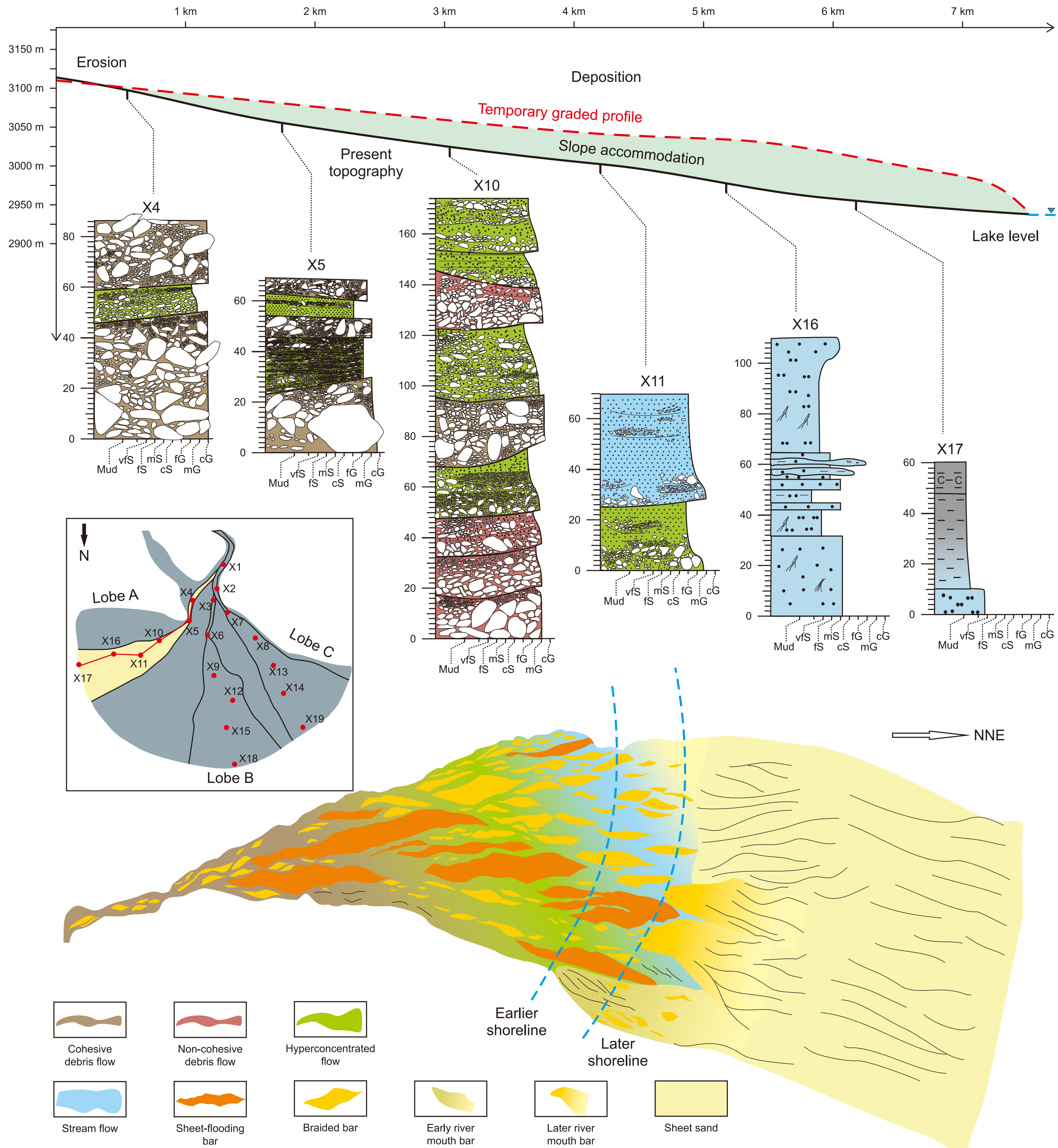

Fig. 3. Topography, sedimentary succession, and facies distribution of the lobe A.

supply. A greater number of bars means more frequent river bifurcations. The channel bifurcation is the primary influence on the widening of the lobe and the width of bars is the secondary.

The width of Lobe B shows a good exponential function with distance. The width of bars shows a trend of slow increase followed by rapid increase with distance. The number of bars shows a tendency to increase slowly and then decrease rapidly (Fig. 6(c)). The width of Lobe B shows a linear relationship with the width of the bars (Fig. 6(d)). This suggests that the width of Lobe B is mainly controlled by the bifurcation of the watercourse upstream, whereas downstream it is mainly the width of the dam body that controls the width of the lobe, illustrating the continued large-scale

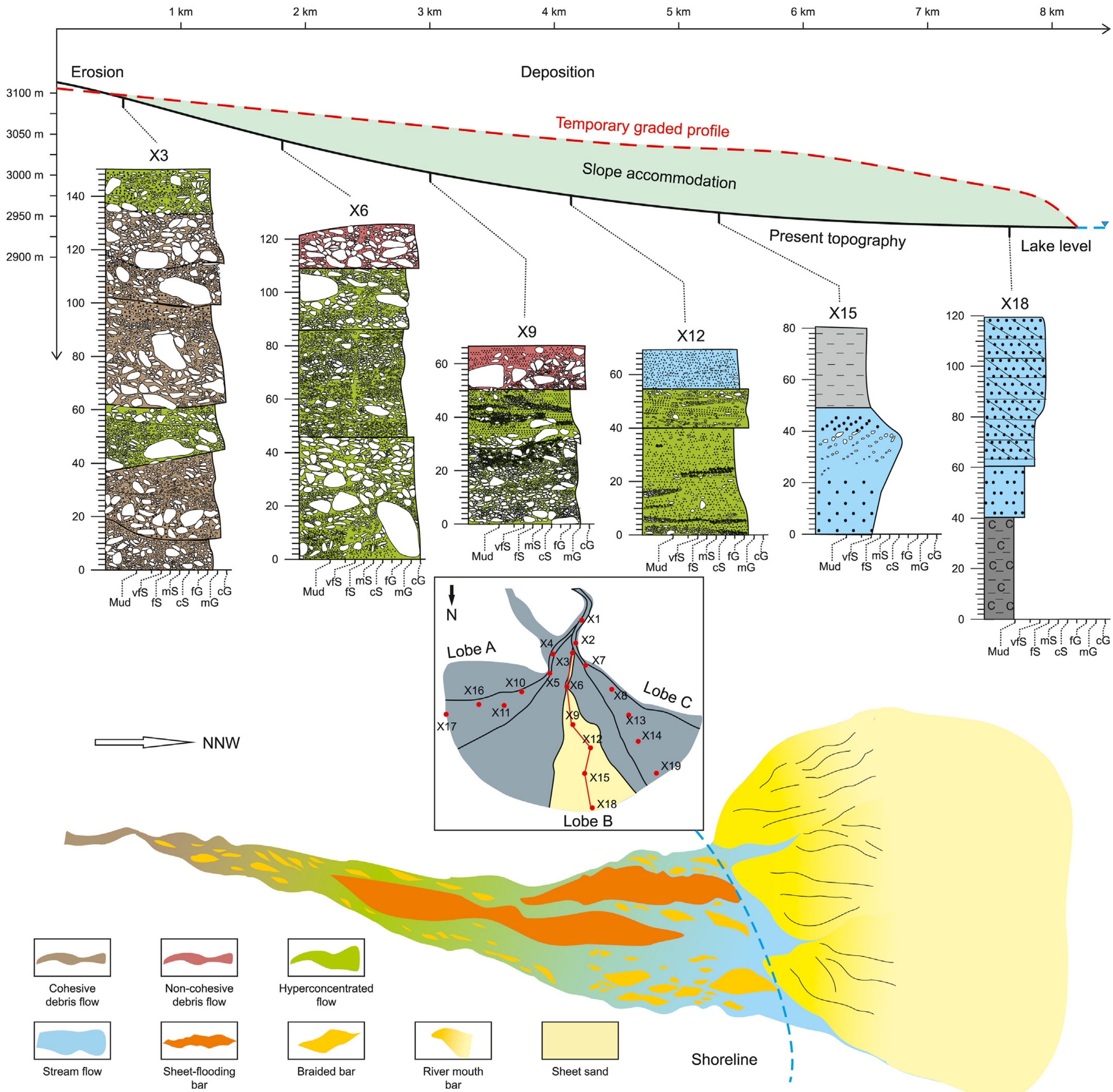

Fig. 4. Topography, sedimentary succession, and facies distribution of the lobe B.

accretion of the mouth bars at the distal end.

The width of Lobe C shows a better polynomial function relationship with the extension distance, indicating the widening rate of the lobe is unstable. The number of bars shows a symmetrical trend of increasing and then decreasing with distance (Fig. 6(e)). The correlation between the width of Lobe C and either the width of the bars or the number of bars is poor, suggesting an abrupt change in topography as the lobe develops (Fig. 6(f)).

In conclusion, the variation of lobe's width is directly controlled by the bifurcation of the channel. When the current is in a supercritical flow state, its bifurcation is not accompanied by sediment unloading, while in a subcritical flow state, it is accompanied by sediment unloading to form a bar, at which time the width of the bar also influences the widening of the lobe to some extent. The smoother and more continuous the fluid change, the better the correlation between the two. Once there is a sudden change in the topography, resulting in a sudden change in fluid velocity and unloading, then the correlation between the two will become worse. The width of the lobe and the width of the bars are fitted with the degree of B > A > C, indicating that that the strength of the influence of the topography on the lobe is C > A > B (Fig. 6).

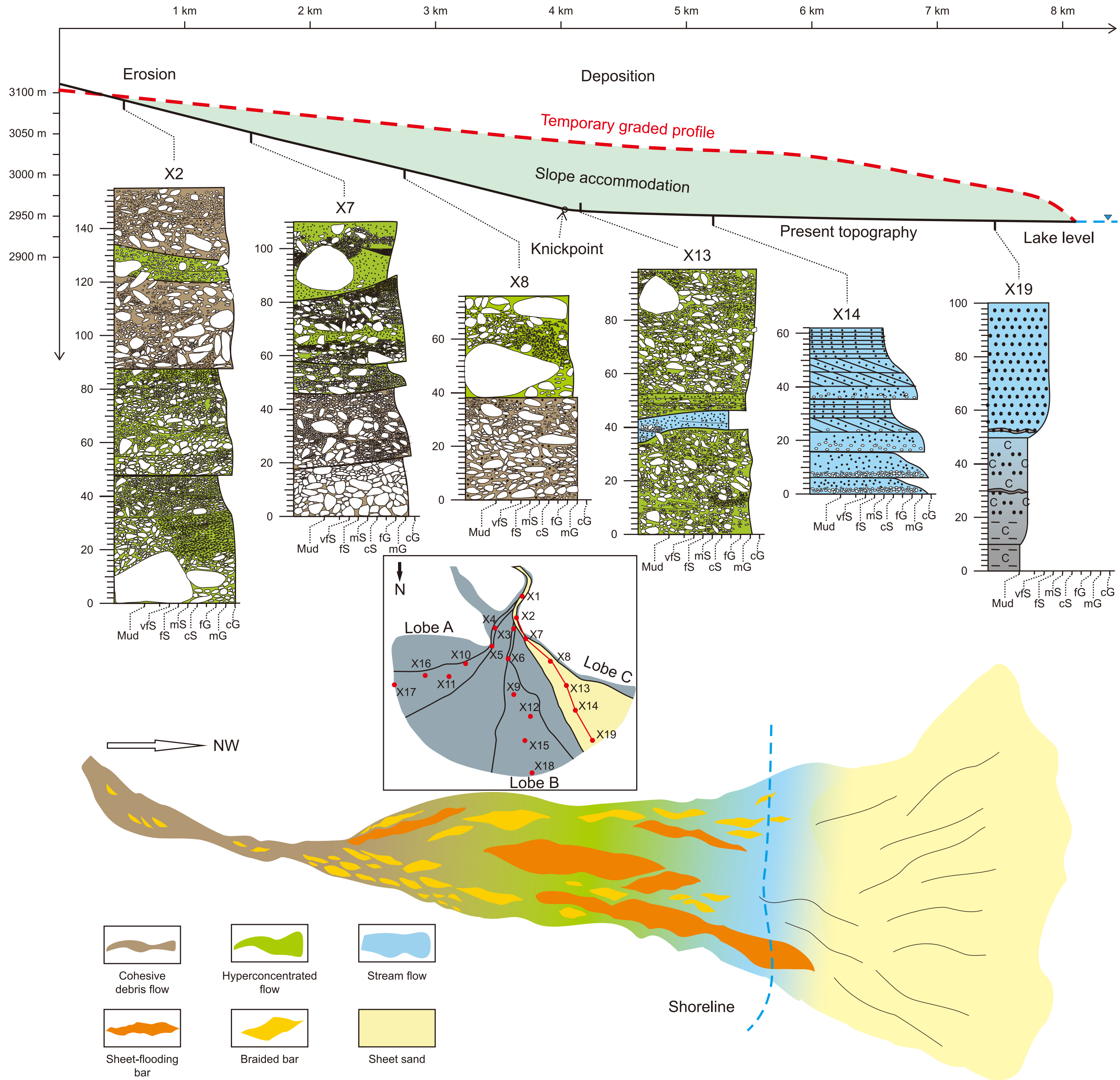

Fig. 5. Topography, sedimentary succession, and facies distribution of the lobe C.

4.3.2. *Proportion of different sediment flows*

Lobe A, B, and C have different proportions of debris flow and HCF development due to the topography in which they were developed. Lobe A has the highest proportion of debris flow and the lowest proportion of hyper-concentrated flow, while Lobe B has the lowest proportion of debris flow and the highest proportion of hyper-concentrated flow (Fig. 7(a)). This suggests that Lobe A is the least controlled by topography, and its hyper-concentrated flow development mainly comes from flow dilution caused by flow power decreasing. Lobe B and C, on the other hand, may come from sudden topographic changes that lead to sediments unloading, thus forcing the flow to shift to hyper-concentrated flow.

In addition, there are two anomalies in the maximum grain size of Lobe B and Lobe C, which are manifested as large gravels suspended in fine gravels, assumed to be remobilized gravels. Other than that, there is little difference in grain size among the three lobes. And due to the sparse data, the grain size is not sufficient to compare the transport capacity of the flows.

5. Discussions

5.1. *Flow transformation*

The fan delta develops debris flow deposit, hyper-concentrated flow deposits and stream flow deposits sequentially from proximal to distal. However, it does not mean that the debris flow is also

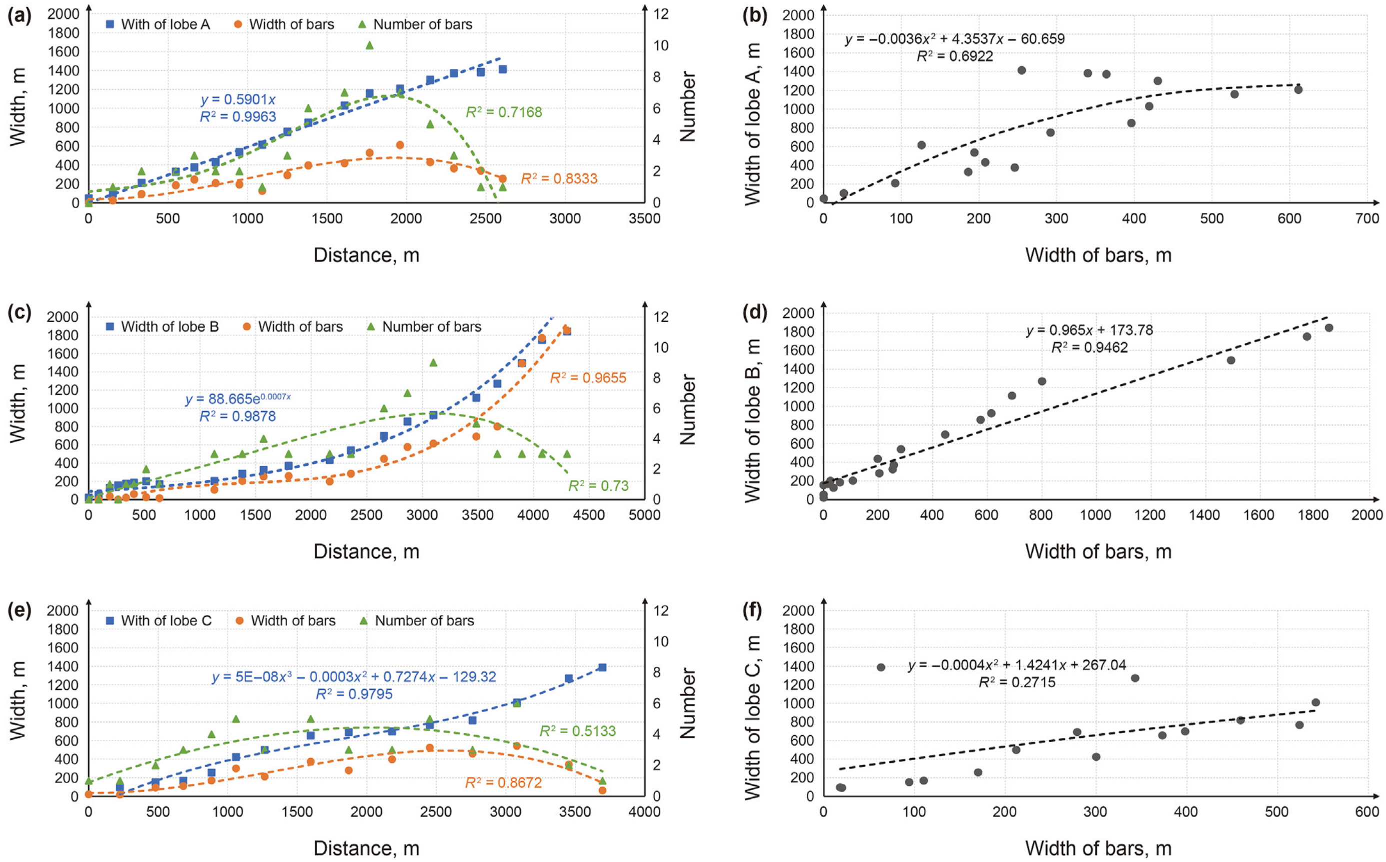

Fig. 6. Parameter fitting relationships for the development of lobes and depositional units.

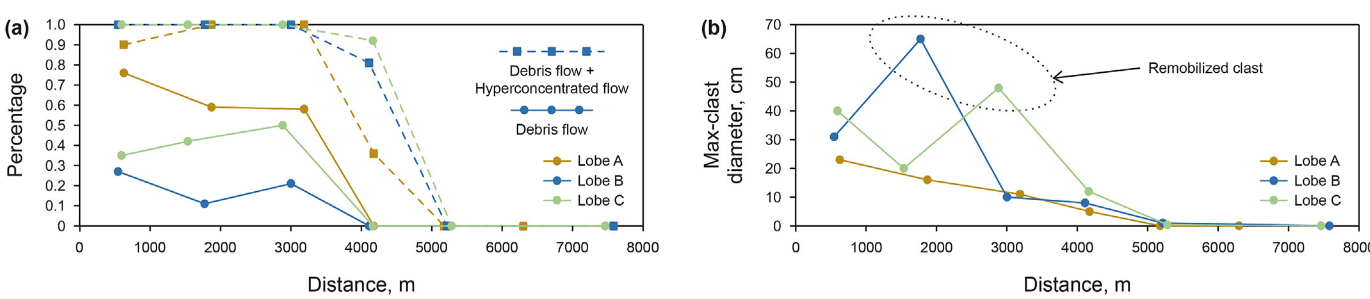

Fig. 7. Statistics of sediment flows proportion **(a)** and gravels with maximum diameter **(b)**.

located in the tail when the fluid is moving. Sohn et al. (1999) proposed two models for the transition of debris flows to hyper-concentrated flow (Fig. 8). The former shifts to hyper-concentrated flow due to dilution of the debris flow (Fig. 8(a and b)), while the latter is due to stagnation of the debris flow deposits (Fig. 8(c and d)). The dilution of the debris flow can be the addition of an external body of water or the unloading of sediments due to a decrease in dispersion pressure (Bagnold, 1954; Hampton, 1972; Rodine and Johnson, 1976; Pierson, 1981; Pierson and Scott, 1985). And there is a process of cohesive debris flow changing to non-cohesive debris flow, which is manifested as matrix-supported gravels changing to sub-horizontally aligned gravels (Rodine and Johnson, 1976; Lowe, 1976; Postma et al., 1983) (Fig. 3, X10; Fig. 8 (b)). This makes the sediments well differentiated spatially. In the latter, the viscous component of the debris flow unloads and the trailing non-viscous component passes over to the front, forming the hyper-concentrated flow (Sohn et al., 1999; Schippa, 2020), which is analogous to the result of regions V and VI in an experimental simulation of a single-event triggered gravity flow carried out by Manica and Schulz (2012), often accompanied by remobilized large gravels from earlier debris flows deposits, with non-cohesive debris flow deposits rarely developed.

The yield strength of debris flow is sufficient to keep gravels in complete suspension (Pierson and Costa, 1987; Coussot and Piau, 1994). And cohesive component is the key factor in determining the yield strength as well as the turbulence of the fluid (Rickenmann, 1991; Blair, 1999). Transformations from debris flow to hyper-concentrated flow is a term referring to yield strength receding and turbulence enhancing, in turn related chiefly to particle concentration and slope gradient (Baas et al., 2009, 2011; De Haas et al., 2015; Le Bouteiller et al., 2020).

Highly turbulent flows bypass obstacles, whereas the viscous

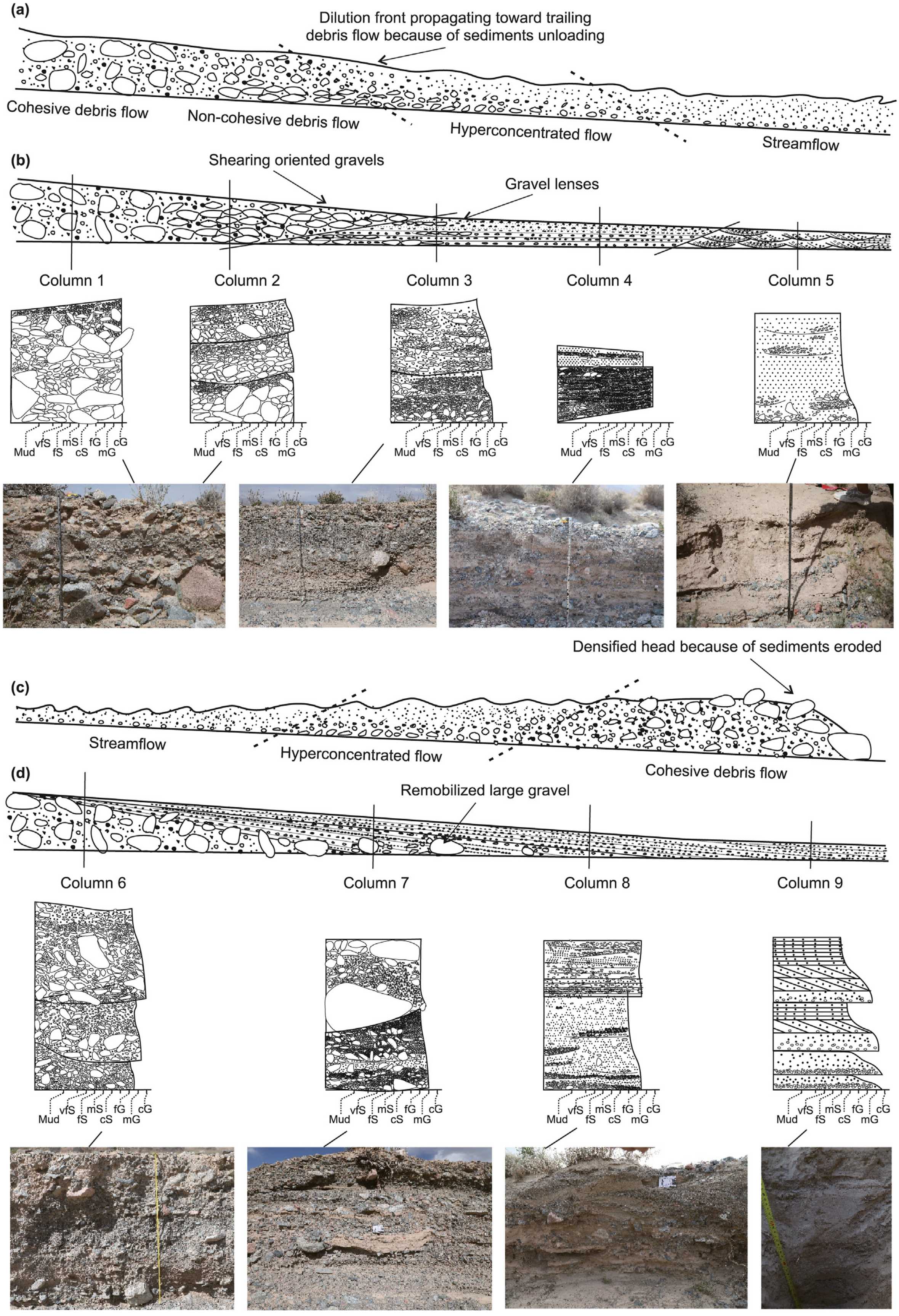

Fig. 8. Comparison of two contrasting styles of debris flow, hyper-concentrated flow, and streamflow events (Modified from Sohn et al., 1999). **(a)** Cohesive debris flow diluting. **(b)** The resultant deposits of diluting model. **(c)** Cohesive debris flow preceding in advance. **(d)** The resultant deposits of preceding.

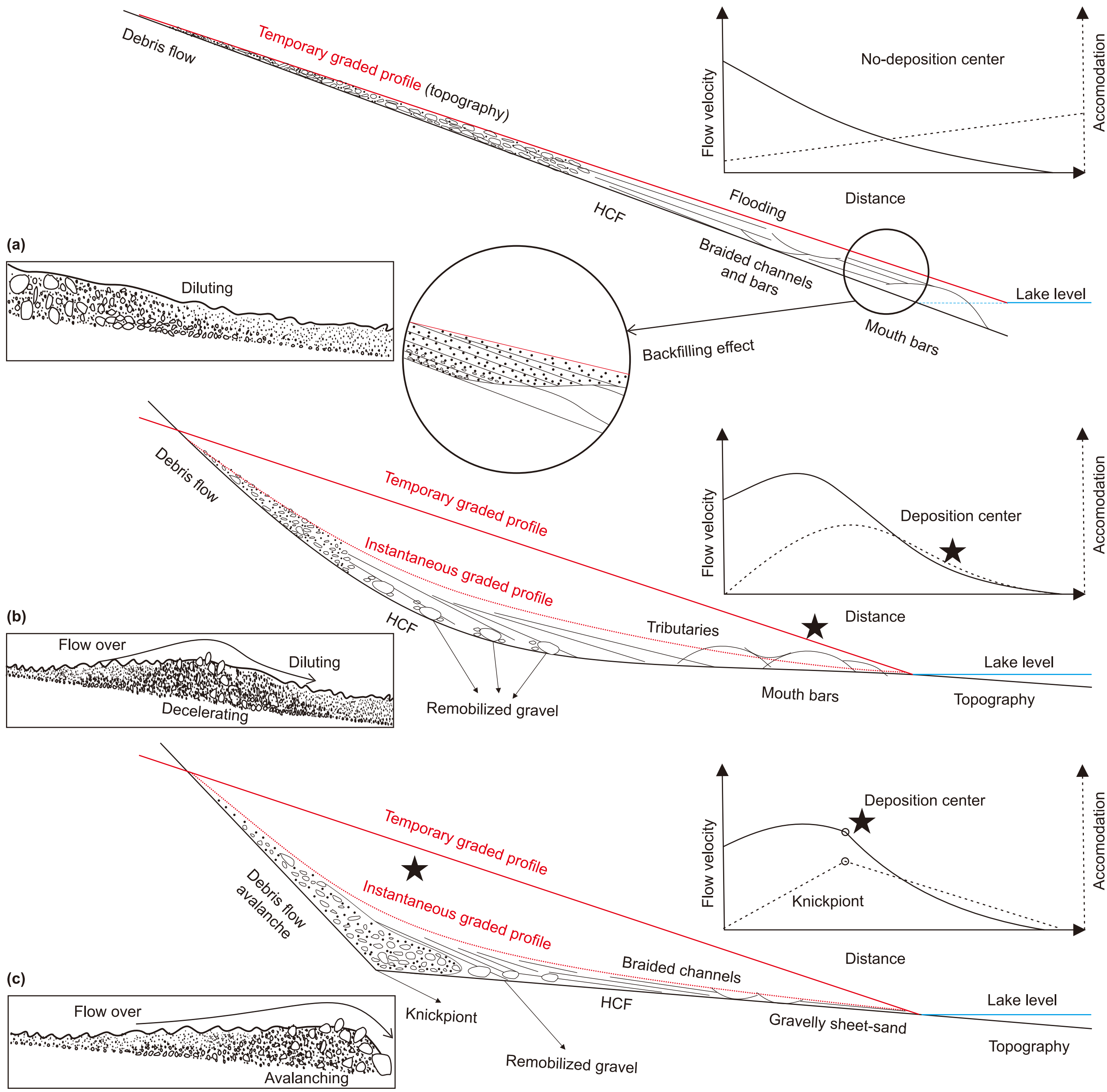

Fig. 9. Sediments flows propagate and transform on different slopes with resultant distribution of sedimentary structures corresponding to the Lobe A **(a)**, Lobe B **(b)** and Lobe C **(c)**, respectively.

component collides with obstacles, leading to a significant reduction in its speed of movement and transport capacity (Postma, 1986; De Haas et al., 2015). The viscous component responds strongly to changes in slope, especially abrupt changes (Kattel et al., 2018). When the topography changes abruptly from steep to gentle after a knickpoint, the viscous component will accumulate first, and the remaining components continue to be transported to form a transitional flow (Fig. 9(c)). When the slope gradient gradually decreases, the viscous component decelerates significantly and the rest of the components overtake it, forming a transitional flow at the front and causing the viscous component diluting (Fig. 9(b)) often accompanied by remobilized large gravels. When the slope is gentle enough and gradient is constant, the viscous component only gradually decelerates, leading to sediments unloading gradually, thus diluting into a transitional flow (Fig. 9(a)). So that, deposition centers develop where there are abrupt changes or the distal part of the topography. And the accommodation of linear slope is evenly distributed from proximal to distal, without distinct deposition center (Fig. 9).

5.2. Backfilling effect and avulsion

Flume experiments show that delta development is controlled by mouth bars (Van Dijk et al., 2009). As the river enters the lake, sediments begin to build up gradually in the upstream direction due to reduced energy. This causes the river level to rise and floods are formed (Clarke et al., 2010). When the lake level drops, sediment supply decreases or upstream hydrodynamics increase, the earlier formed mouth bars will be eroded or modified (Ganti et al., 2014; Ganti et al., 2016; Chadwick et al., 2020, 2021, 2022). Backfilling flooding may promote dilution of the head of the sediments flow and accelerate the transition of debris flow to hyper-concentrated flow. At the same time, due to the blockage of the flooding water, the sediments flow tends to migrate laterally, forming cross trough-like bedding hyper-concentrated flow deposits (Fig. 4). Topography of lobe B makes it easier for sediment to be transported to the distal to form mouth bars, and at the same time, backfilling flooding is enhanced by the effect of mouth bars, which ultimately changes the topography towards lobe A (Fig. 9(b)). Instead of mouth bars, sheet sand developed on lobe A, allowing for the development of many braided bars or sheet-flooding bars upstream (Figs. 3 and 9(a)). Topography of lobe A makes it “most susceptible to transitioning from the backwater avulsion regime to the high–sediment-load modulated avulsion regime with changes in magnitude and duration of floods as well as sediment supply (Brooke et al., 2022). The lack of mouth bars makes backfilling flooding almost non-existent in Lobe C, being dominated by avulsion instead, contributing to the development of braided channels.

5.3. Topography and graded profile

Sequences are stratigraphic stacking patterns formed by cyclical changes in accommodation and sediment supply (Catuneanu et al., 2009, 2011). And sediment supply may fluctuate due to allogenic and autogenic factors (Catuneanu and Zecchin, 2013). Autogenic factors are those controls progradation and retrogradation with no regards to relative sea-level changes and climate (Einsele et al., 1991; Catuneanu and Zecchin, 2013), such as the switching of delta lobes due to the diversion of river mouths (Elliott, 1975; Pulham, 1989). It is clear that lobe switching is a result of the interaction between sediment distribution and topography. Each time the lobe stops, it is a hydrodynamic equilibrium which is consistent with the definition of graded profile (Cross, 1994; Cross and Lessenger, 1998). This interaction is reflected in the fact that topographic slope controls the sediment flows' energy and transformation, which in turn cause erosion or deposition of sediments (Moore and Burch, 1986; Guo et al., 2022). The spatial distribution of sediments and the style of sedimentary structures are the result of the interaction between the bed and the sediment flows (Shields, 1936; Church, 2006; Sebille et al., 2020). Changes in lake level affect the graded profile by changing the elevation of sediment transport, which is the difference of gravitational potential energy ΔE_p (Fig. 10).

Sea level and lake level are proxies for base level (Schumm, 1993). But for subaerial environment, graded profile has been used (Leopold and Bull, 1979; Butcher, 1990). As a lake fan delta, the base level and accommodation of XLG fan delta need to be determined using the lake level and the graded profile, which is the equilibrium surface between erosion and deposition (Cross, 1994; Cross and Lessenger, 1998). Sediment supply, as well as transformation in sediment flows and even topography can also affect the graded profiles (Blum and Valastro, 1989; Blum and Törnqvist, 2000; Van Heijst M and Postma, 2001) (Fig. 9). This implies that the geometries of the graded profiles are instantaneously determined by the topography. Each time the construction of sedimentary lobes stops, the graded profile reaches a new equilibrium. The instantaneous graded profile is a hydrodynamic equilibrium profile and temporary graded profile is an end of depositional trend, which are corresponding to short-term base level and long-term base level defined by Catuneanu (2019). The instantaneous graded profile is the result of a trade-off between sedimentary transport dynamics and resistance, while the temporary graded profile is a response to lake level on a longer time scale. The base level affects the evolution of graded profiles at a long-term scale (Catuneanu, 2019). The ultimate graded profile and base level will overlap (Blum and Törnqvist, 2000). From this point of view, Lobe C, Lobe B and Lobe A sequentially correspond to the evolution process of fan delta development, through debris avalanching under conditions of high slope relief with a knickpoint, reduced gradients by sediment unloading with cohesive debris flow transforming to non-cohesive debris flow, and finally developing widespread unconfined channels (Prior and Bornhold, 1990; Gao et al., 2020) (Fig. 9(c–b, a)).

5.4. Calculation for graded profile

‘Base level’ or graded profile is a surface of equilibrium which sedimentary processes strive to attain, at which neither erosion nor deposition takes place (Barrell, 1917). Therefore, graded profile can be understood as a virtual topography on which the driving and resisting forces of sediment transport are balanced in different kinds of sediment flows. In theory, Navier-Stokes equations can be used to accurately calculate the dynamic changes of sedimentary flows on arbitrary topography (Brakenhoff et al., 2020), but there

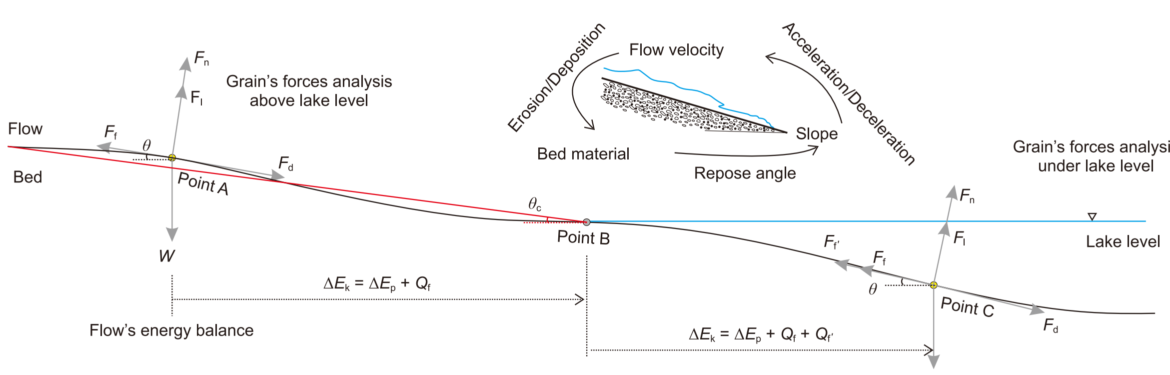

ΔE_k is the difference of kinetic energy. ΔE_p is the difference of gravitational potential energy. Q_f is the internal energy. $Q_{f'}$ is the internal energy underwater.

Fig. 10. A schematic diagram of forces analysis on the particle and the energy conversion during transport above and below the lake level.

are many difficulties in solving the equation (Jerolmack and Mohrig, 2005).

In order to characterize the process of sediment erosion, transport and deposition that leads topography to an equilibrium profile, the better way is to analyze forces of grain on topographic bed under the impact of traction current above lake level (Yen, 2002; Hunter et al., 2007; Allen, 2012; Yu et al., 2022), Five forces are involved in the process (Giménez-curto and Corniero, 2009; Allen, 2012; Clark et al., 2017, Fig. 10).

① Immersed weight: $W = \frac{\pi}{6}D^3(\rho_s - \rho_w)g$,downthrust
② Lift force: $F_l = C_l A D^2 \frac{\rho_w u^2}{2}$,upthrust
③ Drag force: $F_d = C_d A D^2 \frac{\rho_w u^2}{2}$,perpendicular to the slope upwards
④ Support force: F_n,perpendicular to the slope upwards
⑤ Resist force: $F_f = \mu F_n$,along the slope upwards

where D is the sediment grain size, ρ_s is the grain density, ρ_w is the sediment flow density, g is the gravitational acceleration, u is the current velocity, μ is the coefficient of friction relating to bed material (De Blasio et al., 2011), C_l is the lifting coefficient, C_d is the dragging coefficient, both of which are related to Re, and A is the coefficient of the impacted area by flow, which is a constant and generally takes the value of $\pi/4$ (Garde and Sethuraman, 1969).

A simple model based on Newton's first and second laws can be established:

$$W\cos\theta = F_l + F_n \tag{1}$$

$$ma = F_d + W\sin\theta - F_f \tag{2}$$

where θ is the slope angle, m is the mass of grain and $= \frac{\pi}{6}D^3\rho_s$, a is the acceleration of grain.

Deduced:

$$\frac{\pi}{6}D^3\rho_s a = C_d A D^2\frac{\rho_w u^2}{2} + \frac{\pi}{6}D^3(\rho_s - \rho_w)g\sin\theta - \mu\left[\frac{\pi}{6}D^3(\rho_s - \rho_w)g\cos\theta - C_l A D^2\frac{\rho_w u^2}{2}\right] \tag{3}$$

Simplified:

$$a = \frac{3}{\pi}(C_d + C_l)A\frac{\rho_w u^2}{\rho_s D} + \frac{\rho_s - \rho_w}{\rho_s}(\sin\theta - \mu\cos\theta)g \tag{4}$$

Eq. (4) shows that sediment transport is controlled by a combination of flow velocity and topographic slope. An equilibrium profile is a balance between sediment, fluid velocity and topographic slope. No erosion nor deposition means $a = 0$, whence:

$$(\sin\theta_c - \mu\cos\theta_c) = -\frac{3}{\pi}(C_d + C_l)A\frac{\rho_w u^2}{D(\rho_s - \rho_w)g} \tag{5}$$

where θ_c is the critical slope angle of graded (equilibrium) profile.

Equation (5) shows that the geometries of graded profiles will change with the transformation of sediment flows, due to different transport modes, on the other hand the slope will have an impact on flow transformation (Hampton, 1972; Weirich, 1989; Blair and Mcpherson, 1994; Huai et al., 2021; Brierley and Fryirs, 2022). For example, in Lobe B, the slope of the terrain is steeper than that of Lobe A. Theoretically, there should be more debris flow development. However, the gradual decrease of the topographic slope leads to the premature change of the debris flow into hyper-concentrated flow (Fig. 9(b)).

One step further, since $a = \frac{du}{dt} = \frac{du}{dx}\frac{dx}{dt} = u\frac{du}{dx}$, Eq. (4) can be rewritten as:

$$u\frac{du}{dx} = \frac{3}{\pi}(C_d + C_l)A\frac{\rho_w u^2}{\rho_s D} + \frac{\rho_s - \rho_w}{\rho_s}(\sin\theta - \mu\cos\theta)g \tag{6}$$

where x is the transport distance.

Make $M = \frac{3}{\pi}(C_d + C_l)A\frac{\rho_w}{\rho_s D}$, $N = \frac{\rho_s - \rho_w}{\rho_s}g$, whence:

$$dx = \frac{u du}{Mu^2 + N(\sin\theta - \mu\cos\theta)} \tag{7}$$

Deduced:

$$x = \int dx = \int\frac{u du}{Mu^2 + N(\sin\theta - \mu\cos\theta)} = \frac{1}{2}\ln\left[Mu^2 + N(\sin\theta - \mu\cos\theta)\right] \tag{7}$$

Eq. (4) shows that transport distance of sediment is a function of flow velocity and topographic slope. From this point of view, the rise and fall of the lake level essentially changes the topography, which in turn affects the transport distance of sediments.

5.5. Lake level impacting on slope accommodation

Slope accommodation is the space between existing sediment surface and the equilibrium depositional surface (the graded profile), typically a fan surface (Smith, 2004; Kneller et al., 2016). Basin accommodation is controlled by shoreline shifting at some extent (Patruno and Helland-Hansen, 2018). Shoreline migration affected the depositional trends and stacking patterns of the strata, through changing transported elevation of sediments, which is actually the total gravitational potential energy (Fig. 10). When sediment is transported near the shoreline, a stable body of water in a lake or sea adds new resistance to sediment transport (Fig. 10). The topography above the water provides the main driving force of sediments transport, and steady body of water provides the main resisting force. When the driving force is greater than the resistance, progradation forms, basin accommodation priorly filled by sediments. And when the driving force is quite weak, slope accommodation priorly filled. So steep slopes are more likely to fill basin accommodation and form progradation stacking pattern (Blum and Törnqvist, 2000; Amy et al., 2004; Stevenson et al., 2013). Besides, the distance of shoreline migration is much larger on gentle slopes than on steep slopes due to base level rising and falling (Ainsworth and Pattison, 1994; Posamentier and Morris, 2000) (Fig. 11(a)), which makes steep slopes less sensitive to shoreline shift on steep topography, due to the small horizontal distance of shoreline migration, it is likely that depositional system will still prograde during lake level rising (Smith and Joseph, 2004). During forced regression, the driving force can exceed critical values, which can trigger erosion, steeper areas eroded preferentially, gentler parts secondarily, ultimately making topography reach a new equilibrium, becoming a new graded profile (Moore and Burch, 1986; Catuneanu, 2006, 2019) (Fig. 11(b, c, d)). Catuneanu (2006) assumed that knickpoints migrate upstream with time, resulting in a landward expansion of the subaerial unconformity (Fig. 11(b and c)) or in a backfill of the landscape to the level of the new graded profile, accompanied by fluvial onlap of the old graded profile (Fig. 11(d)). However, for alluvial system—fan delta, knickpoints in case d (Fig. 11(d)) will migrate downstream with time, resulting in erosion upstream and depositing downstream, forming a progradation pattern to the level of the new gentler graded profile. In case c (Fig. 11(c)), his choice of a

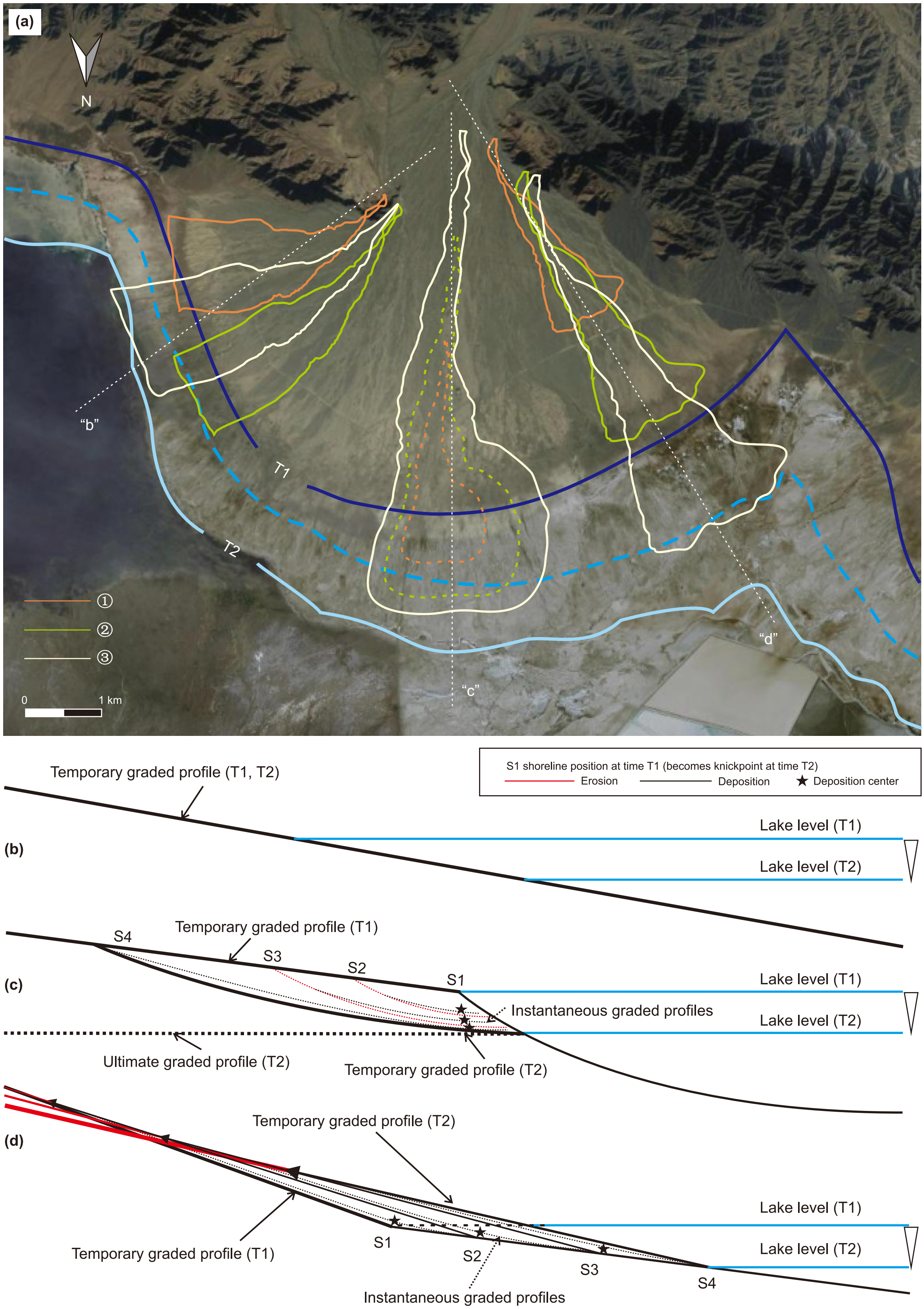

Fig. 11. A conceptual model of the effect and feedback of different topographies on shoreline shifting and lobes stacking pattern during forced base level falling. **(a)** Horizonal shoreline shifting and lobes stacking. **(b)** Alluvial bypass, **(c)** alluvial incision and **(d)** alluvial progradation represent Lobe A, Lobe B and Lobe C respectively (modified from Catuneanu, 2006, Fig. 3.31; Blum and Törnqvist, 2000; Catuneanu, 2019).

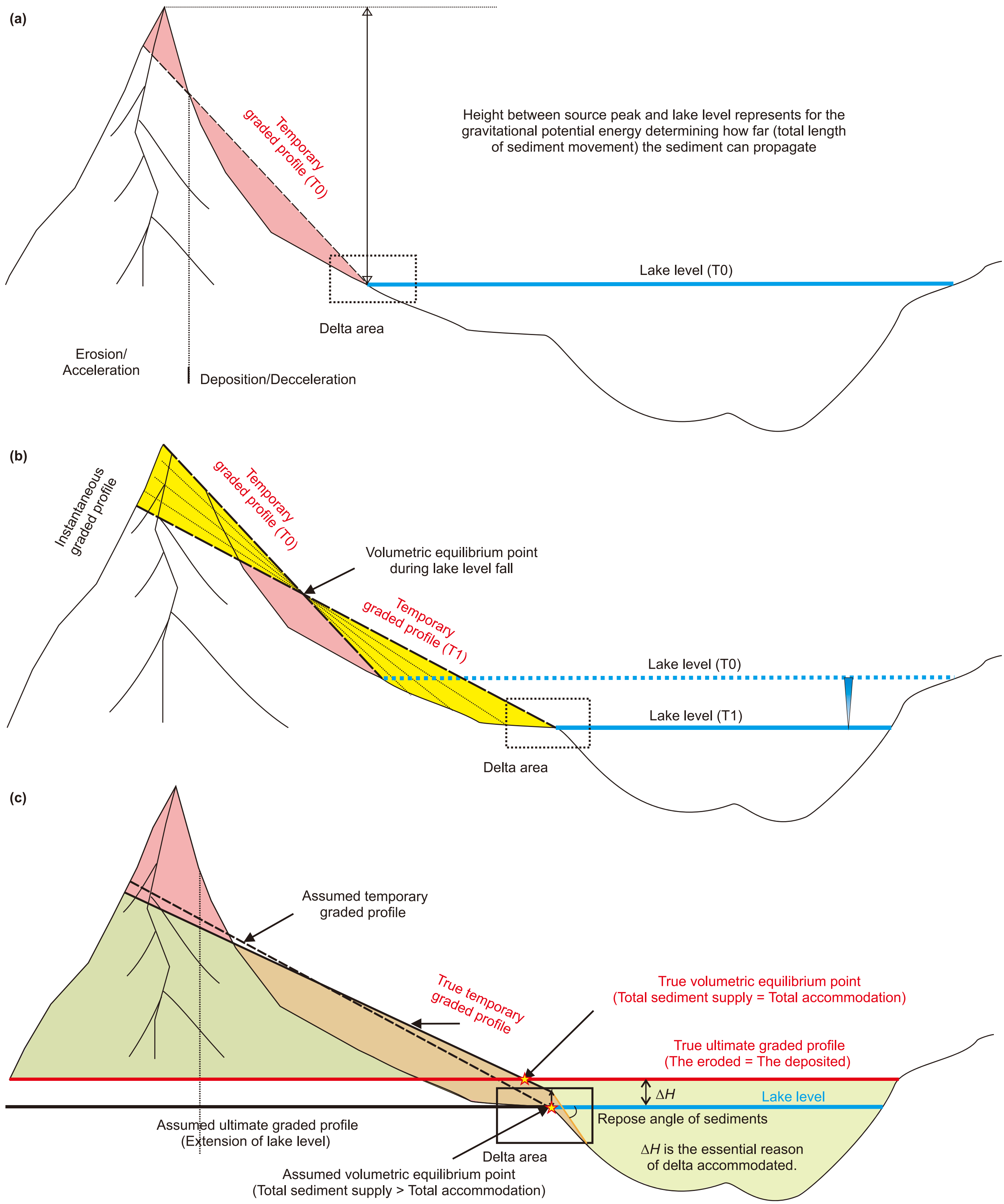

Fig. 12. Schematic illustration of graded profile evolution for a lake basin. **(a)** Graded profile and lake level at T0. **(b)** Graded profile evolution from T0 to T1. **(c)** The difference between assumed graded profiles and true graded profiles.

temporary graded profile (T2) is very arbitrary. The graded profile for period T2 is steeper than that for period T1, and there should be a higher landform which makes the instantaneous graded profile stable enough for a certain length of time to be called a temporary graded profile.

5.6. Graded profile evolution

The ultimate base level is usually seen as the sea level, but temporary base levels exist before the ultimate base level is reached. Fluctuations in the temporary (or instantaneous) base level (or graded profile) result in units and surfaces of sedimentology (instantaneous graded profile or bedsets), or units and surfaces of sequence stratigraphy (temporary graded profile or system tracts) (Zecchin and Catuneanu, 2012; Catuneanu, 2019). The instantaneous graded profile is determined by sediment transport dynamics and resistance, which can be described by Eq. (5). While the temporary graded profile is a response to lake level on a longer time scale which can attributed to the height between the source peak and lake level. What causes the fluctuations is the initial hydrodynamics of sediments flows, which can be attributed to climate. Depositional system is naturally inclined to prograde due to the hydrodynamic equilibrium of graded profile, as the clinoforms of instantaneous graded profiles shown in Fig. 12. While the lake level determines the location of the shoreline, and thus where the depositional system begins to mainly develop, forming either progradation or retrogradation (Fig. 12(b)). It is worth noting that retrogradation can only be caused by lake level rise, whereas progradation can be driven by hydrodynamics of graded profile or lake level fall.

For a lake basin, the evolution of its filling has resulted in a gradual evolution of the topography of the basin margin region from steep to gentle. In the early period, debris flows were more developed on the steep slopes, and the lake level rise and fall had a weaker effect on the stacking pattern of the depositional systems. In the late period, the topography was gentler, and the change of lake level had a stronger control on the stacking pattern of the depositional systems. In terms of periods of geological history, the pattern of stratigraphic sequences has been more strongly influenced by topography than by changes in lake level. Some of the progradation may be the result of steeper topography, even though the lake level was rising at this time. This topographic influence on the evolution of the lake basin troubles the stratigraphic division (Fig. 12). How to eliminate this effect when making system tract divisions is crucial for high resolution stratigraphy sequence.

In addition, the traditional view that the graded profile intersects the lake level at the shoreline implies that there is no accommodating space (Fig. 12(b); Blum and Törnqvist, 2000; Catuneanu, 2019). So how does a delta form? This is clearly contrary to the idea of normal recession of lake level. In fact, the graded profile intersects the lake level at a point of volumetric equilibrium, where the total supply volume equals the total accommodation volume (Fig. 12(c)). When the total supply is greater than the total accommodation, volumetric equilibrium point should be a certain height above the shoreline so that the total eroded volume equals the deposited volume, vice versus. The height is the error produced by the lake level instead of the base level and is the reason why deltas can exist. When the total supply is less than the total accommodation, deltas can temporarily develop due to the hydrodynamics of graded profile. For marine sequences, the influence of topography and hydrodynamics of graded profile are less than the change in sea level. But for lake basin sequences, maybe they are greater than the change in lake level.

6. Conclusions

(1) There are two types of debris-flow deposits: matrix-supported floating conglomerates and clast-supported orientated shearing conglomerates, which correspond to cohesive and non-cohesive debris flows, respectively. The hyper-concentrated flow deposits consist of fining upward remobilized large gravels associated with trough-like interbedded medium gravels and stratified medium to fine gravels. Stream flow, on the other hand, is mainly distinguished by the presence or absence of trough cross bedding fine gravels and sands.

(2) The transformation in sediment flow is controlled both by sediment unloading and topography. Sediments unloading gradually reduces the viscosity of the debris flow, diluting it and shifting it towards hyper-concentrated flow and stream flow. In contrast, topography is controlled by the sudden change of the slope, where the viscous component of the debris flow settles and the less viscous component forms a new flow regime which is hyper-concentrated flow. The latter hyper-concentrated flow leaps over the debris flow and carries early debris flow deposits downstream, which is the most significant difference between the two modes.

(3) An equilibrium profile is a balance between sediment, fluid velocity and topographic slope. The geometries of graded profiles will change with the transformation of sediment flows, due to different transport modes, on the other hand the slope will have an impact on flow transformation. Sediment transport is controlled by a combination of flow velocity and topographic slope, and transport distance is a function of flow velocity and topographic slope. From this point of view, the rise and fall of the lake level essentially changes the topography, which in turn affects the transport distance of sediments.

(4) Topography influenced the dynamics of sediment transport, and the graded profile was an equilibrium between dynamics and resistance of sediment transport. The instantaneous graded profile and temporary graded profile are different scales of equilibrium corresponding to hydrodynamic equilibrium and depositional trend (graded profile evolution) respectively. Besides, basin evolution makes slopes change from steep to gentle, which makes the stacking pattern of sediment is more and more sensitive to lake level changes. Some of the progradation in early stage may be the result of steeper topography, even though the lake level was rising at this time. This topographic influence on the evolution of the lake basin troubles the stratigraphic division. How to eliminate this effect when making system tract divisions is crucial for high resolution stratigraphy sequence.

CRediT authorship contribution statement

Hong-Wei Sun: Writing – review & editing, Writing – original draft, Methodology, Investigation, Formal analysis, Data curation, Conceptualization. **Shun-Li Li:** Methodology, Investigation, Funding acquisition. **Pan Li:** Investigation, Funding acquisition. **Chao-Fan Wei:** Investigation. **Zhan-Teng Wu:** Investigation. **Long-Jv Hai:** Investigation.

Declaration of competing interest

The authors declare the following financial interests/personal relationships which may be considered as potential competing interests: Shun-Li reports financial support was provided by Natural Science Foundation of China. Shun-Li reports financial support was provided by National Key R&D Program of China. Pan Li reports financial support was provided by Research Institute of Petroleum Exploration and Development. If there are other authors, they declare that they have no known competing financial interests or personal relationships that could have appeared to influence the work reported in this paper.

Acknowledgements

This work was funded by the Natural Science Foundation of China (42272124), the National Key R&D Program of China (2023YFF0804302), and Quantitative anatomy of shallow fan deltas in western China project directed by Research Institute of Petroleum Exploration and Development (2020D-5008-03). Thanks for the support. There is no interest conflict of authors.

References

Ainsworth, R.B., Pattison, S.A.J., 1994. Where have all the lowstands gone? Evidence for attached lowstand systems tracts in the Western Interior of North America. Geology 22, 415–418. https://doi.org/10.1130/0091-7613(1994)022<0415:WHATLG>2.3.CO;2.

Allen, P.A., 2008. From landscapes into geological history. Nature 451, 274–276. https://doi.org/10.1038/nature06586.

Allen, J., 2012. Principles of Physical sedimentology. Springer Science & Business Media, pp. 55–80. https://doi.org/10.1007/978-1-4613-2545-1.

Allen, P.A., 2017. Sediment Routing Systems: the Fate of Sediment from Source to Sink. Cambridge University Press, pp. 1–185. https://doi.org/10.1017/9781316135754.

Amy, L.A., McCaffrey, W.D., Kneller, B.C., 2004. The Influence of a Lateral Basin-Slope on the Depositional Patterns of Natural and Experimental Turbidity Currents, vol. 221. Geological Society, London, Special Publications, pp. 311–330. https://doi.org/10.1144/GSL.SP.2004.221.01.17.

Baas, J.H., Best, J.L., Peakall, J., et al., 2009. A phase diagram for turbulent, transitional, and laminar clay suspension flows. J. Sediment. Res. 79 (4), 162–183. https://doi.org/10.2110/jsr.2009.025.

Baas, J.H., Best, J.L., Peakall, J., 2011. Depositional processes, bedform development and hybrid bed formation in rapidly decelerated cohesive (mud–sand) sediment flows. Sedimentology 58 (7), 1953–1987. https://doi.org/10.1111/j.1365-3091.2011.01247.x.

Baas, J.H., Best, J., Peakall, J., 2021a. Rapid gravity flow transformation revealed in a single climbing ripple. Geology 49 (5), 493–497. https://doi.org/10.1130/G48181.1.

Baas, J.H., Niall, D.T., Peakall, J., 2021b. Sole marks reveal deep-marine depositional process and environment: implications for flow transformation and hybrid-event-bed models. J. Sediment. Res. 91 (9), 986–1009. https://doi.org/10.2110/jsr.2020.104.

Bagnold, R.A., 1954. Experiments on a Gravity-free Dispersion of Large Solid Spheres in a Newtonian Fluid under Shear, vol. 225. Royal Society of London Proceedings, ser. A, pp. 49–63. https://doi.org/10.1098/rspa.1954.0186.

Bahrami, S., Aghda, S.M.F., Bahrami, K., et al., 2015. Effects of weathering and lithology on the quality of aggregates in the alluvial fans of Northeast Rivand, Sabzevar, Iran. Geomorphology 241, 19–30. https://doi.org/10.1016/j.geomorph.2015.03.028.

Barrell, J., 1917. Rhythms and the measurements of geological time. Geol. Soc. Am. Bull. 28, 745–904. https://doi.org/10.1130/GSAB-28-745.

Beverage, J.P., Culbertson, J.K., 1964. Hyperconcentrations of suspended sediment. J. Hydraul. Div. 90 (6), 117–128. https://doi.org/10.1061/JYCEAJ.0001424.

Blair, T.C., 1999. Cause of dominance by sheetflood vs. debris-flow processes on two adjoining alluvial fans, Death Valley, California. Sedimentology 46, 1015–1028. https://doi.org/10.1046/j.1365-3091.1999.00261.x.

Blair, T.C., McPherson, J.G., 1994. Alluvial fans and their natural distinction from rivers based on morphology, hydraulic processes, sedimentary processes, and facies assemblages. J. Sediment. Res. 64 (3a), 450–489. https://doi.org/10.1306/D4267DDE-2B26-11D7-8648000102C1865D.

Blair, T.C., McPherson, J.G., 2009. Processes and forms of alluvial fans. In: Parsons, A.J., Abrahams, A.D. (Eds.), Geomorphology of Desert Environments. Springer, Dordrecht, pp. 413–467. https://doi.org/10.1007/978-1-4020-5719-9_14.

Blum, M.D., Törnqvist, T.E., 2000. Fluvial responses to climate and sea-level change: a review and look forward. Sedimentology 47, 2–48. https://doi.org/10.1046/j.1365-3091.2000.00008.x.

Blum, M.D., Valastro, S., 1989. Response of the Pedernales River of central Texas to late Holocene climatic change. Ann. Assoc. Am. Geogr. 79 (3), 435–456. https://doi.org/10.1111/j.1467-8306.1989.tb00271.x.

Brakenhoff, L., Schrijvershof, R., van der Werf, J., et al., 2020. From ripples to large-scale sand transport: the effects of bedform-related roughness on hydrodynamics and sediment transport patterns in delft3d. J. Mar. Sci. Eng. 8 (11), 892. https://doi.org/10.3390/jmse8110892.

Brenna, A., Surian, N., Ghinassi, M., et al., 2020. Sediment–water flows in mountain streams: recognition and classification based on field evidence. Geomorphology 371, 107413. https://doi.org/10.1016/j.geomorph.2020.107413.

Brierley, G., Fryirs, K., 2022. Truths of the Riverscape: moving beyond command-and-control to geomorphologically informed nature-based river management. Geoscience Letters 9 (1), 1–26. https://doi.org/10.1186/s40562-022-00223-0.

Brooke, S., Chadwick, A.J., Silvestre, J., et al., 2022. Where rivers jump course. Science (New York, N.Y.) 376 (6596), 987–990. https://doi.org/10.1126/science.abm1215.

Bull, W.B., 1964. Geomorphology of segmented alluvial fans in western Fresno County, California. US Prof pap 352-E 89–129.

Butcher, S.W., 1990. The knickpoint concept and its implications regarding onlap to the stratigraphic record. Quantitative dynamic stratigraphy 375–385.

Catuneanu, O., 2006. Principles of Sequence stratigraphy[M]. Newnes, pp. 73–163.

Catuneanu, O., 2019. Model-independent sequence stratigraphy. Earth Sci. Rev. 188, 312–388. https://doi.org/10.1016/j.earscirev.2018.09.017.

Catuneanu, O., Zecchin, M., 2013. High-resolution sequence stratigraphy of clastic shelves II: controls on sequence development. Mar. Petrol. Geol. 39 (1), 26–38. https://doi.org/10.1016/j.marpetgeo.2012.08.010.

Catuneanu, O., Abreu, V., Bhattacharya, J.P., et al., 2009. Towards the standardization of sequence stratigraphy. Earth Sci. Rev. 92 (1–2), 1–33. https://doi.org/10.1016/j.earscirev.2008.10.003.

Catuneanu, O., Galloway, W.E., Kendall, C.G.S.C., et al., 2011. Sequence stratigraphy: methodology and nomenclature. Newsl. Stratigr. 44 (3), 173e245.

Chadwick, A.J., Lamb, M.P., 2021. Climate-change controls on river delta avulsion location and frequency. J. Geophys. Res.: Earth Surf. 126 (6), e2020JF005950. https://doi.org/10.1029/2020JF005950.

Chadwick, A.J., Lamb, M.P., Ganti, V., 2020. Accelerated river avulsion frequency on lowland deltas due to sea-level rise. Proc. Natl. Acad. Sci. USA 117 (30), 17584–17590. https://doi.org/10.1073/pnas.1912351117.

Chadwick, A.J., Steele, S., Silvestre, J., et al., 2022. Effect of sea-level change on river avulsions and stratigraphy for an experimental lowland delta. J. Geophys. Res.: Earth Surf. 127 (7), e2021JF006422. https://doi.org/10.1029/2021JF006422.

Chen, H.X., Zhang, L.M., 2015. Edda 1.0: integrated simulation of debris flow erosion, deposition and property changes. Geosci. Model Dev. (GMD) 8 (3), 829–844. https://doi.org/10.5194/gmd-8-829-2015.

Chen, L.Z., Ding, W.G., Geng, Y.Y., et al., 2016. Dynamic change trend of desertification in dulan county during 1975—2015. Desert and Oasis Meteorology 10 (5), 64–71 (in Chinese).

Church, M., 2006. Bed material transport and the morphology of alluvial river channels. Annu. Rev. Earth Planet Sci. 34, 325–354. https://doi.org/10.1146/annurev.earth.33.092203.122721.

Clark, A.H., Shattuck, M.D., Ouellette, N.T., et al., 2017. Role of grain dynamics in determining the onset of sediment transport. Physical Review Fluids 2 (3), 034305. https://doi.org/10.1103/PhysRevFluids.2.034305.

Clarke, L., Quine, T.A., Nicholas, A., 2010. An experimental investigation of autogenic behaviour during alluvial fan evolution. Geomorphology 115 (3–4), 278–285. https://doi.org/10.1016/j.geomorph.2009.06.033.

Coussot, P., Piau, J.M., 1994. On the behavior of fine mud suspensions. Rheol. Acta 33, 175–184. https://doi.org/10.1007/BF00437302.

Cross, T.A., 1994. High-resolution stratigraphic correlation from the perspective of base-level cycles and sediment accommodation. In: Proceedings of Northwestern European Sequence Stratigraphy Congress, vol. 123.

Cross, T.A., Lessenger, M.A., 1998. Sediment volume partitioning: rationale for stratigraphic model evaluation and high-resolution stratigraphic correlation. In: Sequence Stratigraphy—Concepts and Application, vol. 8. Norwegian Petroleum Society Special Publication, pp. 171–195.

De Blasio, F.V., Breien, H., Elverhøi, A., 2011. Modelling a cohesive-frictional debris flow: an experimental, theoretical, and field-based study. Earth Surf. Process. Landforms 36 (6), 753–766. https://doi.org/10.1002/esp.2101.

De Haas, T., Braat, L., Leuven, J.R., et al., 2015. Effects of debris flow composition on runout, depositional mechanisms, and deposit morphology in laboratory experiments. J. Geophys. Res.: Earth Surf. 120 (9), 1949–1972. https://doi.org/10.1002/2015JF003525.

Einsele, G., Ricken, W., Seilacher, A., 1991. Cycles and Events in Stratigraphy. Springer-Verlag, Berlin, p. 955.

Elliott, T., 1975. The sedimentary history of a delta lobe from a Yoredale (Carboniferous) cyclothem. Yorkshire Geological Society, Proceedings 40 (4), 505–536. https://doi.org/10.1144/pygs.40.4.505.

Enos, P., 1991. Flow regimes in debris flow. Deep-Water Turbidite Systems 79–88. https://doi.org/10.1002/9781444304473.ch5.

Evangelinos, D., Nelson, C.H., Escutia, C., et al., 2017. Late Quaternary climatic control of Lake Baikal (Russia) turbidite systems: implications for turbidite systems worldwide. Geology 45 (2), 179–182. https://doi.org/10.1130/G38163.1.

Fonnesu, M., Felletti, F., Haughton, P.D., et al., 2018. Hybrid event bed character and distribution linked to turbidite system sub-environments: the North Apennine Gottero Sandstone (north-west Italy). Sedimentology 65 (1), 151–190. https://doi.org/10.1111/sed.12376.

Ganti, V., Chu, Z., Lamb, M.P., et al., 2014. Testing morphodynamic controls on the location and frequency of river avulsions on fans versus deltas: huanghe (Yellow River), China. Geophys. Res. Lett. 41 (22), 7882–7890. https://doi.org/10.1002/2014GL061918.

Ganti, A.J.V., Chadwick, H.J., Hassenruck-Gudipati, B.M., et al., 2016. Experimental

river delta size set by multiple floods and backwater hydrodynamics. Sci. Adv. 2, e1501768. https://doi.org/10.1126/sciadv.1501768.
Gao, C.L., Ji, Y.L., Wu, C.L., et al., 2019. Facies and depositional model of alluvial fan dominated by episodic flood events in arid conditions: an example from the Quaternary Poplar Fan, north-western China. Sedimentology 67 (4), 1750–1796. https://doi.org/10.1111/sed.12684.
Gao, C.L., Ji, Y.L., Jin, J., et al., 2020. Sedimentary characteristics and evolution model of fluvial alluvial fan controlled by paroxysmal flood: a case study of modern aspen alluvial fan on the northern margin of Heshituoluogai basin. Acta Pet. Sin. 41 (3), 310–328. https://doi.org/10.7623/syxb202003006 (in Chinese).
Garde, R.J., Sethuraman, S., 1969. Variation of the drag coefficient of a sphere rolling along a boundary. La Houille Blanche 55 (7), 727–732. https://doi.org/10.1051/lhb/1969057.
Geleynse, N., Storms, J.E., Walstra, D.J.R., et al., 2011. Controls on river delta formation; insights from numerical modelling. Earth Planet Sci. Lett. 302 (1–2), 217–226. https://doi.org/10.1016/S1270-9638(99)80023-6.
GIMÉNEZ-CURTO, L.A., Corniero, M.A., 2009. Entrainment threshold of cohesionless sediment grains under steady flow of air and water. Sedimentology 56 (2), 493–509. https://doi.org/10.1111/j.1365-3091.2008.00981.x.
Guo, J.X., Jiang, Z.X., Xie, X.Y., et al., 2021. Deep-lacustrine sediment gravity flow channel-lobe complexes on a stepped slope: an example from the Chengbei Low Uplift, Bohai Bay Basin, East China. Mar. Petrol. Geol. 124, 104839. https://doi.org/10.1016/j.marpetgeo.2020.104839.
Guo, J., Cui, Y.F., Xu, W.J., et al., 2022. Numerical investigation of the landslide-debris flow transformation process considering topographic and entrainment effects: a case study. Landslides 19, 773–788. https://doi.org/10.1007/s10346-021-01791-6.
Hampton, M.A., 1972. The role of subaqueous debris flow in generating turbidity currents. J. Sediment. Res. 42 (4), 775–793.
Harvey, A., 2011. Dryland Alluvial Fans. Arid Zone Geomorphology: Process, Form and Change in Drylands, pp. 333–371.
Harvey, A.M., Mather, A.E., Stokes, M., 2005. Alluvial fans: geomorphology, sedimentology, dynamics—introduction. In: A Review of Alluvial-Fan Research. Geological Society, London, Special Publications, pp. 1–7. https://doi.org/10.1144/GSL.SP.2005.251.01.01, 251(1).
Heward, A.P., 1978. Alluvial fan and lacustrine sediments from the stephanian A and B (La magdalena, cinera—matallana and sabero) coalfields, northern Spain. Sedimentology 25 (4), 451–488. https://doi.org/10.1111/j.1365-3091.1978.tb02076.x.
Hjulström, F., 1935. *Studies of the morphological activity of rivers as illustrated by the River Fyris.* Doctoral dissertation. The Geological institution of the University of Upsala.
Holmes, A., 1945. Principles of physical geology. Geol. Foren. Stockh. Forh. 67 (1), 115–116. https://doi.org/10.1080/11035894509446436.
Huai, W.X., Li, S., Katul, G.G., et al., 2021. Flow dynamics and sediment transport in vegetated rivers: a review. J. Hydrodyn. 33 (3), 400–420. https://doi.org/10.1007/s42241-021-0043-7.
Hunter, N.M., Bates, P.D., Horritt, M.S., et al., 2007. Simple spatially-distributed models for predicting flood inundation: a review. Geomorphology 90 (3–4), 208–225. https://doi.org/10.1016/j.geomorph.2006.10.021.
Hussain, A., Haughton, P.D.W., Shannon, P.M., et al., 2020. High-resolution X-ray fluorescence profiling of hybrid event beds: implications for sediment gravity flow behaviour and deposit structure. Sedimentology 67 (6), 2850–2882. https://doi.org/10.1111/sed.12722.
Jerolmack, D.J., Mohrig, D., 2005. A unified model for subaqueous bed form dynamics. Water Resour. Res. 41 (12). https://doi.org/10.1029/2005WR004329.
Johnson, A.M., 1970. Mobilization of debris flows. Zeitschrift fur Geomorphologie (Annals of geomorphology). Supplement 9, 168–186.
Johnson, A.M., 1984. Debris flows. Slope Instability, pp. 257–361.
Kataoka, K., Nakajo, T., 2004. Flow transformation and depositional organization of debris flow-hyperconcentrated flow-streamflow spectrum in volcanic fan-delta setting the Pleistocene Lower and Middle Formations, Yachiho Group, central Japan. Journal of the Sedimentological Society of Japan 59 (59), 17–26. https://doi.org/10.4096/jssj1995.59.17.
Kattel, P., Kafle, J., Fischer, J.T., et al., 2018. Interaction of two-phase debris flow with obstacles. Eng. Geol. 42, 197–217. https://doi.org/10.1016/j.enggeo.2018.05.023.
Kneller, B., Dykstra, M., Fairweather, L., et al., 2016. Mass-transport and slope accommodation: implications for turbidite sandstone reservoirs. AAPG Bull. 100 (2), 213–235. https://doi.org/10.1306/09011514210.
Kvale, E.P., Bowie, C.M., Flenthrope, C., et al., 2020. Facies variability within a mixed carbonate–siliciclastic sea-floor fan (upper Wolfcamp Formation, Permian, Delaware Basin, New Mexico). AAPG (Am. Assoc. Pet. Geol.) Bull. 104 (3), 525–563. https://doi.org/10.1306/06121917225.
Lane, E.W., 1953. Progress report on studies on the design of stable channels by the bureau of reclamation. Proc. Am. Soc. Civ. Eng. 79 (9), 1–31. https://doi.org/10.1061/(ASCE)EM.1943-7889.0001980.
Leopold, L.B., Bull, W.B., 1979. Base level, aggradation, and grade. Proc. Am. Phil. Soc. 123 (3), 168–202.
Lewis, D.W., Laird, M.G., Powell, R.D., 1980. Debris flow deposits of early Miocene age, Deadman stream, Marlborough, New Zealand. Sediment. Geol. 27 (2), 83–118. https://doi.org/10.1016/0037-0738(80)90032-9.
Le Bouteiller, C., Chambon, G., Naaim-Bouvet, F., et al., 2020. Hydraulics and rheology of natural hyperconcentrated flows from Draix-Bleone observatory, French Alps. J. Hydraul. Res. 59 (2), 181–195. https://doi.org/10.1080/00221686.2020.1744750.
Li, S.L., Zhu, X.M., Liu, Q.H., et al., 2017a. Evaluation and prediction of favorable reservoirs in source-to-sink systems of the palaeogene, shaleitian uplift. Earth Sci. 6 (11), 1994–2009. https://doi.org/10.3799/dqkx.2017.127 (in Chinese).
Li, S.L., Zhu, X.M., Li, H.Y., Liu, Q.H., et al., 2017b. Quantitative characterization of elements and coupling mode in source-to-sink system: a case study of the Shahejie Formation between the Shaleitian uplift and Shanan sag, Bohai sea. China Offshore Oil Gas 29 (4), 39–50. https://doi.org/10.11935/j.issn.1673-1506.2017.04.005 (in Chinese).
Lowe, D.R., 1976. Subaqueous liquefied and fluidized sediment flows and their deposition. Sedimentology 23, 258–308. https://doi.org/10.1111/j.1365-3091.1976.tb00051.x.
Lowe, D.R., 1979. Sediment gravity flows: their classification and some problems of application to natural flows and deposits. In: Geology of Continental Slopes, vol. 27. SEPM Special publication, Tulsa, pp. 75–82.
Lowe, D.R., 1982. Sediment gravity flows; II, Depositional models with special reference to the deposits of high-density turbidity currents. J. Sediment. Res. 52 (1), 279–297. https://doi.org/10.1306/212F7F31-2B24-11D7-8648000102C1865D.
Luo, Y.N., Wang, Y.J., 2017. Analysis of climate change and possible impacts on ecological environment in Wulan County in the last 35 years. Qinghai Environment 27 (3), 131–139 (in Chinese).
Lv, S.C., 2018. Study on Lake Carbon Pool Effect in Qinghai Lake and Xiligou Lakes. Qinghai Normal University, Qinghai, pp. 11–21 (in Chinese).
Manica, R., Schulz, H.E., 2012. Sediment gravity flows: study based on experimental simulations. Hydrodynamics-Natural Water Bodies 1, 263–286. https://doi.org/10.5772/28794.
Milana, J.P., Ruzycki, L., 1999. Alluvial-fan slope as a function of sediment transport efficiency. J. Sediment. Res. 69, 553–562. https://doi.org/10.2110/jsr.69.553.
Milana, J.P., Tietze, K.W., 2002. Three-dimensional analogue modelling of an alluvial basin margin affected by hydrological cycles: processes and resulting depositional sequences. Basin Res. 14, 237–264. https://doi.org/10.1046/j.1365-2117.2002.00188.x.
Moore, I.D., Burch, G.J., 1986. Modelling erosion and deposition: topographic effects. Transactions of the ASAE 29 (6), 1624–1630. https://doi.org/10.13031/2013.30363.
Nelson, C.H., Escutia, C., Goldfinger, C., et al., 2009. External controls on modern clastic turbidite systems: three case studies. In: Kneller, B., Martinsen, O.J., McCaffrey, B. (Eds.), External Controls on Deep-Water Depositional Systems, vol. 92. SEPM Special Publication, Society for Sedimentary Geology, pp. 57–76. https://doi.org/10.2110/sepmsp.092.057.
Nemec, W., 1990. Aspects of sediment movement on steep delta slopes. Coarse-grained deltas 10 (2), 29–73.
Nemec, W., Muszyński, A., 1982. Volcaniclastic alluvial aprons in the Tertiary of Sofia district (Bulgaria). In: *Annales Societatis Geologorum Poloniae*., 52. pp. 239–303 No. 1-4.- Reference Edited.
Nemec, W., Steel, R.J., 1984. Alluvial and Coastal Conglomerates: Their Significant Features and Some Comments on Gravelly Mass-Flow Deposits, pp. 1–31.
Nota, P.J., Zhang, X., Liu, H., et al., 2024. Effects of upstream and downstream boundary conditions on lacustrine shallow-water delta morphologies: a numerical modeling approach. Mar. Petrol. Geol. 167, 106966. https://doi.org/10.1016/j.marpetgeo.2024.106966.
Parker, G., Paola, C., Whipple, K.X., et al., 1998. Alluvial fans formed by channelized fluvial and sheet flow. I: theory. J. Hydraul. Eng. 124 (10), 985–995. https://doi.org/10.1061/(ASCE)0733-9429(1998)124:10(985.
Patruno, S., Helland-Hansen, W., 2018. Clinoforms and clinoform systems: review and dynamic classification scheme for shorelines, subaqueous deltas, shelf edges and continental margins. Earth Sci. Rev. 185, 202–233. https://doi.org/10.1016/j.earscirev.2018.05.016.
Pierson, T.C., 1981. Dominant particle support mechanisms in debris flows at Mt Thomas, New Zealand, and implications for flow mobility. Sedimentology 28 (1), 49–60. https://doi.org/10.1111/j.1365-3091.1981.tb01662.x.
Pierson, T.C., Costa, J.E., 1987. A rheologic classification of subaerial sediment-water flows. Rev. Eng. Geol. 7, 1–12.
Pierson, T.C., Scott, K.M., 1985. Downstream dilution of a lahar: transition from debris flow to hyperconcentrated streamflow. Water Resour. Res. 21 (10), 1511–1524. https://doi.org/10.1029/WR021i010p01511.
Posamentier, H.W., Morris, W.R., 2000. Aspects of the stratal architecture of forced regressive deposits. In: Hunt, D., Gawthorpe, R.L. (Eds.), Sedimentary Responses to Forced Regressions, vol. 172. Geological Society of London, Special Publication, pp. 19–46. https://doi.org/10.1144/GSL.SP.2000.172.01.02.
Postma, G., 1986. Classification for sediment gravity-flow deposits based on flow conditions during sedimentation. Geology 14, 291–294. https://doi.org/10.1130/0091-7613(1986)14%3C291:CFSGDB%3E2.0.CO;2.
Postma, G., 1990. Depositional architecture and facies of river and fan deltas: a synthesis. Coarse-grained deltas, 13-27. https://doi.org/10.1002/9781444303858.ch2.
Postma, G., Roop, Th B., Ruegg, G.J.H., 1983. Sandy-gravelly mass flow deposits in an ice-marginal lake (Saalian, Leuvenumsche Beek Valley, Veluwe, The Netherlands), with emphasis on plug-flow deposits. Sediment. Geol. 34, 59–82. https://doi.org/10.1016/0037-0738(83)90035-0.
Postma, G., Nemec, W., Kleinspehn, K.L., 1988. Large floating clasts in turbidites: a mechanism for their emplacement. Sediment. Geol. 58 (1), 47–61. https://doi.org/10.1016/0037-0738(88)90005-X.
Prior, D.B., Bornhold, B.D., 1990. The underwater development of Holocene fan deltas. Coarse-grained deltas 75–90. https://doi.org/10.1002/9781444303858.ch4.

Pulham, A.J., 1989. Controls on internal structure and architecture of sandstone bodies within Upper Carboniferous fluvial-dominated deltas, County Clare, western Ireland. In: Whateley, M.K.G., Pickering, K.T. (Eds.), Deltas: Sites and Traps for Fossil Flues, vol. 41. Geological Society, Special Publication, p. 179e203. https://doi.org/10.1144/GSL.SP.1989.041.01.14.

Reading, H.G., Richards, M., 1994. Turbidite systems in deep-water basin margins classified by grain size and feeder system. AAPG (Am. Assoc. Pet. Geol.) Bull. 78, 792–822. https://doi.org/10.1306/A25FE3BF-171B-11D7-8645000102C1865D.

Rickenmann, D., 1991. Hyperconcentrated flow and sediment transport at steep slopes. J. Hydraul. Eng. 117 (11), 1419–1439. https://doi.org/10.1061/(ASCE)0733-9429(1991)117:11(1419.

Rodine, J.D., Johnson, A.M., 1976. The ability of debris, heavily freighted with coarse clastic materials, to flow on gentle slopes. Sedimentology 23, 213–234. https://doi.org/10.1111/j.1365-3091.1976.tb00047.x.

Schippa, L., 2020. Modeling the effect of sediment concentration on the flow-like behavior of natural debris flow. Int. J. Sediment Res. 35 (4), 315–327. https://doi.org/10.1016/j.ijsrc.2020.03.001.

Schumm, S.A., 1993. River response to baselevel change: implications for sequence stratigraphy. J. Geol. 101 (2), 279–294. https://doi.org/10.1086/648221.

Sebille, E.V., Aliani, S., Law, K.L., et al., 2020. The physical oceanography of the transport of floating marine debris. Environ. Res. Lett. 15 (2), 023003. https://doi.org/10.1088/1748-9326/ab6d7d.

Shanmugam, G., 2020. Gravity flows: types, definitions, origins, identification markers, and problems: gravity lows. Journal of The Indian Association of Sedimentologists (peer reviewed) 37 (2), 61–90. https://doi.org/10.51710/jias.v37i2.117.

Shi, M.Z., Xiao, L.G., 2003. An analysis of climatic hazards in Wulan County. Qinghai Meteorology (4), 5.

Shields, A., 1936. Application of similarity principles and turbulence research to bed-load movement. Soil Conservation Service.

Smith, R.D.A., 2004. In: Lomas, S., Joseph, P. (Eds.), Silled Sub-basins to Connected Tortuous Corridors; Sediment Distribution Systems on Topographically Complex Sub-aqueous Slopes, vol. 222. Geological Society of London Special Publication, pp. 23–43.

Smith, R., Joseph, P., 2004. Onlap stratal architectures in the Gres d'Annot: geometric models and controlling factors. Geological Society, London, Special Publications 221 (1), 389–399. https://doi.org/10.1144/GSL.SP.2004.221.01.21.

Sohn, Y.K., Rhee, C.W., Kim, B.C., 1999. Debris flow and hyperconcentrated flood-flow deposits in an alluvial fan, northwestern part of the Cretaceous Yongdong Basin, Central Korea. J. Geol. 107, 111–132. https://doi.org/10.1086/314334.

Steel, R.J., 1974. New red sandstone floodplain and piedmont sedimentation in the hebridean province, scotland. J. Sediment. Res. 44 (2), 336–357. https://doi.org/10.1306/74D72A27-2B21-11D7-8648000102C1865D.

Sternberg, H., 1875. Untersuchungen uber langen-und querprofil geschiebefuhrender flusse. Zeitschrift fur Bauwesen XXV, 483–506.

Stevenson, C.J., Talling, P.J., Wynn, R.B., et al., 2013. The flows that left no trace: very large-volume turbidity currents that bypassed sediment through submarine channels without eroding the sea floor. Mar. Petrol. Geol. 41, 186–205. https://doi.org/10.1016/j.marpetgeo.2012.02.008.

Takahashi, T., 1978. Mechanical characteristics of debris flow. J. Hydraul. Div. 104 (8), 1153–1169. https://doi.org/10.1061/JYCEAJ.0005046.

Takahashi, T., 1981. Debris flow. Annu. Rev. Fluid Mech. 13 (1), 57–77. https://doi.org/10.1146/annurev.fl.13.010181.000421.

Tinterri, R., Civa, A., Laporta, M., et al., 2020. Turbidites and turbidity currents. In: Regional Geology and Tectonics. Elsevier, pp. 441–479. https://doi.org/10.1016/B978-0-444-64134-2.00016-X.

Uhrin, A., Sztanó, O., 2012. Water-level changes and their effect on deepwater sand accumulation in a lacustrine system: a case study from the Late Miocene of western Pannonian Basin, Hungary. Int. J. Earth Sci. 101 (5), 1427–1440. https://doi.org/10.1007/s00531-011-0741-4.

Van Dijk, M., Postma, G., Kleinhans, M.G., 2009. Autocyclic behaviour of fan deltas: an analogue experimental study. Sedimentology 56 (5), 1569–1589. https://doi.org/10.1111/j.1365-3091.2008.01047.x.

Van Heijst, M., Postma, G., 2001. Fluvial response to sea-level changes: a quantitative analogue, experimental approach. Basin Res. 13 (3), 269–292. https://doi.org/10.1046/j.1365-2117.2001.00149.x.

Wasson, R.J., 1977. Last-glacial alluvial fan sedimentation in the lower derwent valley, tasmania. Sedimentology 24 (6), 781–799. https://doi.org/10.1111/j.1365-3091.1977.tb01915.x.

Weirich, F.H., 1989. The generation of turbidity currents by subaerial debris flows, California. Geol. Soc. Am. Bull. 101 (2), 278–291. https://doi.org/10.1130/0016-7606(1989)101<0278:TGOTCB>2.3.CO;2.

Whipple, K.X., Parker, G., Paola, C., et al., 1998. Channel dynamics, sediment transport, and the slope of alluvial fans: experimental study. J. Geol. 106, 677–694. https://doi.org/10.1086/516053.

Woolway, R.I., Kraemer, B.M., Lenters, J.D., et al., 2020. Global lake responses to climate change. Nat. Rev. Earth Environ. 1, 388–403. https://doi.org/10.1038/s43017-020-0067-5.

Wu, Z.S., Zhang, G.G., Liang, Z.X., et al., 2017. Influence of particle shape and medium on sediment repose angle. Yellow River 39 (3), 24–27.

Yang, T., Cao, Y.C., Liu, K.Y., et al., 2020. Gravity-flow deposits caused by different initiation processes in a deep-lake system. AAPG (Am. Assoc. Pet. Geol.) Bull. 104 (7), 1463–1499. https://doi.org/10.1306/03172017081.

Yen, B.C., 2002. Open channel flow resistance. J. Hydraul. Eng. 128 (1), 20–39. https://doi.org/10.1061/(ASCE)0733-9429(2002)128:1(20.

Yu, X.H., Li, S.L., Sun, H.W., 2022. Coupling effect of "mass-slope"from source to sink in clastic rock deposition. J. Palaeogeogr. 24 (6), 1037–1057. https://doi.org/10.7605/gdlxb.2022.06.075 (in Chinese).

Zavala, C., 2020. Hyperpycnal (over density) flows and deposits. J. Palaeogeogr. 9 (1), 17. https://doi.org/10.1186/s42501-020-00065-x.

Zecchin, M., Catuneanu, O., 2012. High-resolution sequence stratigraphy of clastic shelves I: units and bounding surfaces. Mar. Petrol. Geol. 39, 1e25. https://doi.org/10.1016/j.marpetgeo.2012.08.015.

Zhang, K., Wu, S., Feng, W., et al., 2021. Experimental study of fan delta evolution: autogenic cycles of fully confined channelized flow and small secondary channelized flows. Sediment. Geol. 426, 106024. https://doi.org/10.1016/j.sedgeo.2021.106024.